

This discussion paper is/has been under review for the journal Atmospheric Chemistry and Physics (ACP). Please refer to the corresponding final paper in ACP if available.

Relating hygroscopicity and optical properties to chemical composition and structure of secondary organic aerosol particles generated from the ozonolysis of α -pinene

C. Denjean^{1,2}, P. Formenti¹, B. Picquet-Varrault¹, E. Pangui¹, P. Zapf¹, Y. Katrib¹, C. Giorio^{3,*}, A. Tapparo³, A. Monod⁴, B. Temime-Roussel⁴, P. Decorse⁵, C. Manganey⁵, and J. F. Doussin¹

¹Laboratoire Interuniversitaire des Systèmes Atmosphériques (LISA), UMR-CNRS 7583, Université Paris-Est-Créteil (UPEC) et Université Paris Diderot (UPD), Institut Pierre Simon Laplace (IPSL), Créteil, France

²Leibniz Institute for Tropospheric Research, Leipzig, Germany

³Dipartimento di Scienze Chimiche, Università degli Studi di Padova, via Marzolo 1, 35131 Padova, Italy

⁴Aix Marseille Université, CNRS, Laboratoire Chimie de l'Environnement (LCE), FRE 3416, 13331 Marseille, France

ACPD

14, 10543–10596, 2014

Relating
hygroscopicity and
optical properties

C. Denjean et al.

Title Page

Abstract

Introduction

Conclusions

References

Tables

Figures

◀

▶

◀

▶

Back

Close

Full Screen / Esc

Printer-friendly Version

Interactive Discussion



⁵ITODYS, Université Paris Diderot, Sorbonne Paris Cité, CNRS UMR 7086, 15 rue J-A de Baïf, 75013 Paris, France

*now at: Department of Chemistry, University of Cambridge, Lensfield road, CB2 1EW Cambridge, UK

Received: 7 March 2014 – Accepted: 10 April 2014 – Published: 28 April 2014

Correspondence to: C. Denjean (denjean@tropos.de)

Published by Copernicus Publications on behalf of the European Geosciences Union.

ACPD

14, 10543–10596, 2014

Relating hygroscopicity and optical properties

C. Denjean et al.

Title Page

Abstract

Introduction

Conclusions

References

Tables

Figures



Back

Close

Full Screen / Esc

Printer-friendly Version

Interactive Discussion



Abstract

Secondary Organic Aerosol (SOA) were generated from the ozonolysis of α -pinene in the CESAM simulation chamber. The formation and ageing of the SOA were studied by following their optical, hygroscopic and chemical properties. The optical properties 5 investigated by determining the particle Complex Refractive Index (CRI). The hygroscopicity was quantified by measuring the effect of RH on particle size (Growth Factor, GF) and scattering coefficient ($f(RH)$). The oxygen to carbon (O : C) atomic ratio of the particle surface and bulk were used as a sensitive parameter to correlate the changes in hygroscopic and optical properties of the SOA composition in CESAM.

10 The real CRI at 525 nm wavelength decreased from 1.43–1.60 (± 0.02) to 1.32–1.38 (± 0.02) during the SOA formation. The decrease in real CRI correlates with a decrease in the O : C ratio of SOA from 0.68 (± 0.20) to 0.55 (± 0.16). In contrast, the GF stayed roughly constant over the reaction time, with values of 1.02–1.07 (± 0.02) at 90 % (± 4.2) RH. Simultaneous measurements of O : C ratio of the particle surface revealed that the 15 SOA was not composed of a homogeneous mixture, but with less oxidised species at the surface which would limit the water adsorption onto particle. In addition, an apparent change of both mobility diameter and scattering coefficient with increasing RH from 0 to 30 % was observed for SOA after 16 h reaction. We postulate that this change could be due to a change in the viscosity of the SOA from a predominantly glassy state 20 to a predominantly liquid state.

1 Introduction

Organic compounds are known to account for a large fraction of atmospheric aerosol, ranging between 20 and 90 % of the total particle mass (Kanakidou et al., 2005). In particular, secondary organic aerosol (SOA), formed by the condensation of gas-phase 25 oxidation products of volatile organic compounds (VOCs), is a major constituent of the total organic aerosol (Turpin and Huntzicker, 1995; Zhang et al., 2007).

Title Page

Abstract

Introduction

Conclusions

References

Tables

Figures

◀

▶

◀

▶

Back

Close

Full Screen / Esc

Printer-friendly Version

Interactive Discussion



SOA typical a diameter ranging between less than ten to several hundreds of nanometers. Particles in this size range have long atmospheric lifetimes and scatter incoming solar radiation. SOA can also change clouds properties by acting as Cloud Condensation Nuclei (CCN) (Saxena et al., 1995; Lohmann and Feichter, 2005; Novakov and Penner, 1993; RiveraCarpio et al., 1996; Matsumoto et al., 1997).

There are large uncertainties in estimating the impact of SOA on climate due to the complexity of the mixtures found in the atmosphere and the limited range of measurements available (Kanakidou et al., 2005). SOA precursors produce a large number of oxidation products (Goldstein and Galbally, 2009), resulting in many possible chemical reaction pathways (de Gouw et al., 2005; Hallquist et al., 2009). In addition, during its residence time in the atmosphere, SOA may undergo several physical and chemical ageing processes altering their chemical composition (Kalberer et al., 2004; Baltensperger, 2005; Yasmeen et al., 2012) and size distribution (Andreae, 2009). As a result, the atmosphere contains many organic compounds with a large variety of structures, chain lengths, functionalities and degrees of oxidation (Kroll and Seinfeld, 2008; Jimenez et al., 2000). Therefore SOA possesses a wide range of hygroscopic and optical properties (Lambe et al., 2013; Suda et al., 2012).

In global climate models, the radiative effect of SOA is currently described by adopting a constant Complex Refractive Index (CRI) and a single size Growth Factor (GF). Depending on the model, the adopted real part of the CRI at visible wavelengths ranges between 1.45 to 1.60 (Kinne et al., 2003; Pere et al., 2011; Zaveri et al., 2010). Some models assumed that SOA absorb weakly solar radiation, and set the imaginary part of the CRI near 0.006, while others ignore the absorption by SOA. Concerning hygroscopic properties, a single size GF of SOA derived from limited available data is used (O'Donnell et al., 2011; Hoyle et al., 2009). Evidence from field measurements shows, however, that the hygroscopic and optical properties of SOA are not static and depend on their origin and transport in the atmosphere (Lang-Yona et al., 2010; Duplissy et al., 2010; Jimenez et al., 2009; Chang et al., 2010; Dinar et al., 2008). Few laboratory investigations have begun to explore the change of SOA properties during their life-

Relating hygroscopicity and optical properties

C. Denjean et al.

[Title Page](#)

[Abstract](#)

[Introduction](#)

[Conclusions](#)

[References](#)

[Tables](#)

[Figures](#)

◀

▶

◀

▶

[Back](#)

[Close](#)

[Full Screen / Esc](#)

[Printer-friendly Version](#)

[Interactive Discussion](#)



Relating hygroscopicity and optical properties

C. Denjean et al.

time. α -pinene ozonolysis is one of the most well studied SOA systems, as α -pinene is a significant biogenic VOC in many regions, and its ozonolysis plays an important role in formation of SOA (Hallquist et al., 2009; Griffin et al., 1999; Yu et al., 1999; Kavouras et al., 1998, 1999). α -pinene- O_3 SOA is also generally considered as a model for many 5 biogenic VOCs containing an endocyclic double bond (Guenther et al., 1995). Saathoff et al. (2003) conducted experiments of α -pinene- O_3 SOA in a simulation chamber and observed an increase of the GF at 90 % RH from 1.080 to 1.106. Cocker et al. (2001) reported also an increase of the GF at 85 % RH from 1.065 to 1.11 within 6 h. In contrast, Warren et al. (2009) and Qi et al. (2010) reported a constant GF at 90 % RH for 10 α -pinene- O_3 SOA over 6 h of reaction. An increase of the real CRI from 1.39 to 1.52 at $\lambda = 532$ nm during formation of the α -pinene- O_3 SOA has been reported by Kim et al. (2013). To date, none of the previous studies have simultaneously determined the hygroscopic and optical properties, and their evolution with the SOA's chemical composition.

To accurately quantify the SOA impacts on climate, it is critical to simultaneously determine the hygroscopic behaviour of its size distribution and optical properties as well as their dependence on the chemical composition. Atmospheric simulation chambers are powerful tools to simultaneously study the physical, chemical, optical and hygroscopic properties of SOA and follow their changes along their lifecycle by simulating their formation and ageing due to oxidation and photolysis in the atmosphere (Meyer et al., 2008; Henry and Donahue, 2012; Tritscher et al., 2011). In this work, we take advantage of the long aerosol lifetime in the CESAM chamber (French acronym for Experimental Multiphasic Atmospheric Simulation Chamber, Wang et al., 2011) to set-up ageing experiments in order to characterise their effect on both optical properties and hygroscopicity. The objective of this paper is to examine the evolution of the hygroscopic and optical properties of α -pinene- O_3 SOA during its formation and to relate these changes to variations in aerosol chemical composition.

Title Page	
Abstract	Introduction
Conclusions	References
Tables	Figures
◀	▶
◀	▶
Back	Close
Full Screen / Esc	
Printer-friendly Version	
Interactive Discussion	



2 Methods

Measurements have been conducted in the humidity-controlled simulation chamber CESAM (Wang et al., 2011), which permits the study of the formation and ageing of SOA over long periods of time, and under various relevant atmospheric conditions.

Experiments were conducted to simultaneously measure different parameters:

- *CRI* at $\lambda = 525\text{ nm}$, a specific wavelength in the mid-visible; the Complex Refractive Index (*CRI*, $m = n - ik$) is an important parameter to link the physical and chemical properties of the SOA and its ability to interact with radiation, allowing a description of the scattering and absorbing characteristics of SOA.
- *GF(RH)*, size growth factor, the ratio of the particle diameter at a given RH to the particle diameter at low RH, for one selected size of particles; this parameter is used to characterise the hygroscopic properties of the SOA and thus, it is an indicator of its ability to act as CCN.
- *f(RH)*, scattering growth factor, the ratio of σ_{scat} at high RH to the σ_{scat} at low RH, for the entire size distribution; this parameter allows the study of the effect of water absorption on the scattering properties of SOA.
- *O:C*, the oxygen-to-carbon ratio, for both the bulk and the surface composition of the SOA; it is well known that particle composition, in particular that of the surface, strongly influences the water uptake ability of the particle and its CCN potential (McFiggans et al., 2006; Dusek et al., 2006; Hatch et al., 2008; Moussa et al., 2009; McIntire et al., 2010; Semeniuk et al., 2007). To encompass the difficulty of representing the full molecular composition, the O:C ratio of SOA has been included in global climate modelling to provide a description of the aerosol ageing (Tost and Pringle, 2012). Furthermore, a number of recent publications have reported a positive correlation between hygroscopicity and bulk O:C ratio for both laboratory and ambient SOA (Massoli et al., 2010; Jimenez et al., 2009; Chang et al., 2010; Duplissy et al., 2011).



2.1 Simulation chamber and associated instruments

CESAM is a 4.2 m^3 cylindrical stainless steel chamber which has been designed to investigate both atmospheric gas-phase and aerosol-phase chemistry. As described in Wang et al. (2011), the wall properties and ventilation system guarantee a long sub-micron particle lifetime in the chamber which enables the study of aerosols for more than 20 h. Water vapour can be directly injected in CESAM and thus the RH of the reaction mixture varied *in situ* from 0 to 100 %.

The basic experimental setup and a schematic view of the CESAM chamber are shown in Fig. 1. Temperature and relative humidity in the chamber are monitored using a Vaisala transmitter equipped with a capacitive thin-film Humicap sensor. The sensor was calibrated prior to the experiments and has a RH accuracy of $\pm 1.9\%$ up to 90 % RH and a temperature accuracy of $\pm 0.1\text{ }^\circ\text{C}$ at $20\text{ }^\circ\text{C}$.

α -pinene, ozone and their reaction products were continuously monitored by a Fourier-Transform InfraRed spectrometer (FTIR) from Bruker GmbH (Ettlingen, Germany) coupled to a multi reflection cell which allows creates an optical path of 192 m. Additionally, ozone was monitored by a commercial Horiba APOA 370 instrument (Kyoto, Japan) with a detection limit of 0.5 ppb and a precision of 0.1 ppb.

The particle number size distribution was measured using a Scanning Mobility Particle Sizer (SMPS including a DMA 3080 and CPC 3010, TSI). The SMPS was operated at flow rates 3/0.3 Lpm (sheath flow/aerosol sample flow). The resulting measured size distribution ranged from 14 to 505 nm. The size calibration of the SMPS was performed using monodisperse PolyStyrene Latex spheres (PSL, Duke Scientific). PSL, with diameters ranging from 100 to 500 nm, were nebulised with a constant output atomiser (TSI model 3075). The measured diameters were found to be larger than the PSL certified diameters (by about 10 % for 100 nm PSL spheres), so a correction factor was applied. Size distributions were corrected by the SMPS software for both the loss by diffusion of particles in the SMPS tubing and the contribution of multicharged particles.

[Title Page](#)[Abstract](#)[Introduction](#)[Conclusions](#)[References](#)[Tables](#)[Figures](#)[◀](#)[▶](#)[◀](#)[▶](#)[Back](#)[Close](#)[Full Screen / Esc](#)[Printer-friendly Version](#)[Interactive Discussion](#)

Relating hygroscopicity and optical properties

C. Denjean et al.

[Title Page](#)

[Abstract](#)

[Introduction](#)

[Conclusions](#)

[References](#)

[Tables](#)

[Figures](#)

[◀](#)

[▶](#)

[◀](#)

[▶](#)

[Back](#)

[Close](#)

[Full Screen / Esc](#)

[Printer-friendly Version](#)

[Interactive Discussion](#)



2.2 Optical properties measurements

The aerosol scattering coefficient (σ_{scat}) was measured using an integrating nephelometer (model M9003, Ecotech). The nephelometer operates at 525 nm wavelength and measures light scattered from particles at angles between 10° and 170°. It also measures temperature at both the sample inlet and within its cell with an accuracy of ±0.6 °C, and the RH within its cell with an accuracy of ±3 %. Prior to each series of experiments, the nephelometer was calibrated using particle-free air and CO₂.

The particle light absorption coefficient (σ_{abs}) was determined by means of an aethalometer (Model AE31, Magee Scientific) operated with several light sources at seven wavelengths, covering the near ultra-violet to the near infrared wavelength range ($\lambda = 370, 470, 520, 590, 660, 880$ and 950 nm). The aethalometer measures the attenuation of the transmitted light through a quartz fibre filter with increasing particle loading. This measurement can suffer from artefacts associated with reactions with oxidants occurring on particles deposited on the surface of the filter and desorption of gaseous compounds from the filter (Weingartner et al., 2003). Thus, a denuder was installed upstream of the aethalometer to remove ozone and VOCs. It has also been observed that the aethalometer can suffer from biases at high RH as a result of the filter taking up water and scattering more light compared with the reference measurement (Cappa et al., 2008; Arnott et al., 2005). Therefore, the aethalometer was not used when the RH in the chamber was above 1 %.

The spectral attenuation coefficient (σ_{attn}) resulting from the attenuation of light through the sampled aerosol deposit on the filter was obtained as:

$$\sigma_{\text{attn}}(\lambda, m) = \frac{A}{Q} \frac{\Delta \text{attn}}{\Delta t} \quad (1)$$

where A is the spot area, Q the volumetric flowrate and Δattn the change in light attenuation during the time interval Δt . It is well known that σ_{attn} obtained with the aethalometer is higher than the true σ_{abs} (Arnott et al., 2005; Bond et al., 1999; Bond and Bergstrom, 2006; Cappa et al., 2008; Collaud Coen et al., 2010; Weingartner et al.,

2003). Various systematic errors need to be corrected. We applied the empirical correction described by Collaud Coen et al. (2010) which includes R , the attenuation effect due to light absorbing particles accumulating on the filter, C_{ref} , the multiple scattering by the filter fibres and α , the scattering correction due to scattering of aerosols embedded in the filter:

$$\sigma_{\text{abs}}(\lambda, m) = \frac{\sigma_{\text{ATTN}}(\lambda, m) - \alpha(\lambda) \cdot \sigma_{\text{scatt}}(\lambda, m)}{C_{\text{ref}} \cdot R} \quad (2)$$

R decreases with the gradual increase of attenuation due to the accumulation of absorbing particles embedded in the filter. As will be shown in the Sect. 3.2., the attenuation modification during SOA measurement was very low, indicating weakly light absorbing particles. Thus, we assumed that R was equal to unity.

C_{ref} can be estimated by comparing σ_{attn} measured with the aethalometer measurements and σ_{abs} obtained from a non-filter based instrument (for example a photoacoustic photometer). However, simultaneous measurements with these two instruments were not possible during the reported experiments. Weingartner et al. (2003) estimated that soot particles coated with α -pinene-O₃ SOA were characterised by $C_{\text{ref}} = 3.64 \pm 0.98$ and 3.90 ± 0.56 at 450 and 660 nm respectively. We used the average $C_{\text{ref}} = 3.77 \pm 2.11$ of these values to correct σ_{attn} in this study.

$\alpha(\lambda)$ was deduced from the σ_{attn} measured by the aethalometer with non-absorbing ammonium sulfate particles according to the method described by Arnott et al. (2005) at the 7-wavelengths of the aethalometer. We used the value of $\alpha(\lambda) = 1.3 \times 10^{-3} \cdot \lambda^{5.6 \times 10^{-1}}$ estimated by Denjean et al. (2014). The values of σ_{scat} at the wavelengths of the aethalometer other than 525 nm were derived from calculations based on Mie theory, measured size distributions and the constant CRI retrieved at 525 nm.

The CRI of SOA was measured under dry conditions ($\text{RH} < 1\%$) at 525 nm by optical closure experiments involving scattering and absorbing coefficients (respectively σ_{scat} and σ_{abs}) measured at 525 nm and the number size distribution. The details of the calculations are given by Denjean et al. (2014). Briefly, σ_{scat} and σ_{abs} were calculated

according to the following equation:

$$\sigma_{\text{scat, abs}}(\lambda, m) = \sum_{D_p} Q_{\text{scat, abs}}(D_p, \lambda, m) \frac{\pi}{4} D_p^2 \left(\frac{dN}{d\log D_p} \right) d\log D_p \quad (3)$$

where D_p is the geometrical particle diameter, $\frac{dN}{d\log D_p}$ the number size distribution and

- 5 $Q_{\text{scat, abs}}(D_p, \lambda, m)$ the scattering and absorption efficiencies. $Q_{\text{scat, abs}}(D_p, \lambda, m)$ were calculated using Mie scattering calculations described by Bohren and Huffman (1983).

The values of σ_{scat} and σ_{abs} of SOA were simultaneously measured and compared with those calculated based on the Mie theory. To allow this comparison, all measured 10 σ_{scat} were corrected from the sample temperature and pressure and from the angular truncation error examined for the nephelometer. The best-guess CRI was determined by minimizing the difference between measured σ_{scat} and σ_{abs} and those obtained using Mie calculations.

2.3 Hygroscopic properties measurements

The hygroscopic properties of SOA were investigated using two complementary approaches: (1) a Hygroscopic Tandem Differential Mobility Analyzer (H-TDMA) used to 15 measure the RH dependency of the particles diameter for single size particles and (2) in-situ experiments within the CESAM chamber that allowed for the measurement of σ_{scat} changes after water uptake for polydisperse aerosol size distribution.

The hygroscopic behaviour of monodisperse SOA was measured with a Hygroscopic 20 Tandem Differential Mobility Analyzer (H-TDMA) described in detail by Denjean et al. (2014). Briefly, the H-TDMA is composed of a DMA (TSI, 3080) that selects an initial mobility diameter under dry conditions $D_{p,m}$ (dry), an aerosol humidifier with a controlled higher RH and a DMA (TSI, 3080) coupled to a CPC (TSI, 3010) to measure the wet size distribution over mobility diameter $D_{p,m}$ (RH). Both DMAs of the H-TDMA 25 were calibrated using monodisperse PSL particles (Duke Scientific) ranging from 100 to 500 nm. A size shift was observed for both DMAs. Details on the data treatment can

Title Page

Abstract

Introduction

Conclusions

References

Tables

Figures

◀

▶

◀

▶

Back

Close

Full Screen / Esc

Printer-friendly Version

Interactive Discussion



be found in Denjean et al. (2014). The particles residence time for humidification is 15 s and corresponds to the residence time in the aerosol humidifier plus the transit time in the second DMA. In this study, the H-TDMA was typically operated at a constant high RH of $90 \pm 1\%$. The hygroscopic size growth factor (GF) describes the relative increase in the geometric diameter of particles due to water uptake at a specific RH:

$$GF(RH) = \frac{D_{p,m}(RH)}{D_{p,m}(\text{dry})} \quad (4)$$

Dry and humidified mobility diameters were obtained by assuming that the size distributions exhibit a lognormal profile. H-TDMA measurements were validated by measuring the humidogram of laboratory generated ammonium sulfate particles. The GF was found to agree with values calculated using the Köhler model (Denjean et al., 2014).

In addition to H-TDMA measurements, the hygroscopic behaviour of polydisperse SOA was measured by exposing the particles *in situ* to increasing humidity in the CESAM chamber. A detailed description of this approach can be found in Denjean et al. (2014). Water vapour produced in a small glass vessel filled with ultrapure water ($18.2 \text{ M}\Omega$, ELGA Maxima) was injected into the chamber where it was mixed using a stainless steel fan. The RH in the chamber increased linearly from 0 to 100 % within approximately 1 h. The change in σ_{scat} due to hygroscopic growth of the overall size distribution was followed with the nephelometer. The ratio of the scattering coefficient at a specific RH $\sigma_{\text{scat}}(RH)$ to the dry scattering coefficient $\sigma_{\text{scat}}(\text{dry})$ give the $f(RH)$:

$$f(RH) = \frac{\sigma_{\text{scat}}(RH)}{\sigma_{\text{scat}}(\text{dry})} \quad (5)$$

During humidification, RH was monitored within the chamber and at the inlet of the nephelometer. With this approach, the residence time for particle humidification was a few minutes which is significantly longer than during H-TDMA measurements. It has been previously shown (Denjean et al., 2014) that the two approaches of hygroscopicity measurements could lead to different results, which carry information on water

Relating hygroscopicity and optical properties

C. Denjean et al.

[Title Page](#)

[Abstract](#)

[Introduction](#)

[Conclusions](#)

[References](#)

[Tables](#)

[Figures](#)

[◀](#)

[▶](#)

[◀](#)

[▶](#)

[Back](#)

[Close](#)

[Full Screen / Esc](#)

[Printer-friendly Version](#)

[Interactive Discussion](#)



transfer dynamics, possible particles reorganisation or phase transfer equilibrium establishment.

2.4 Aerosol sampling and chemical composition analysis

A High Resolution time-of-flight aerosol mass spectrometer (HR-ToF-AMS, Aerodyne) (DeCarlo et al., 2006) was used to determine the bulk composition of organic aerosols (Aiken et al., 2007, 2008). The instrument was used under standard conditions (vaporiser at 600 °C and electron ionisation at 70 eV). StandardAMS calibration procedures using NH₄NO₃ particles were performed throughout the campaign and included Ionisation Efficiency (IE) calibration using Brute Force Single Particle (BFSP) method at 350 nm particle mobility diameter as well as size calibration using 6 DMA-selected dried particle sizes over the range of interest 100–350 nm. Single ion calibration as well as baseline and threshold were analysed prior each experiment.

The HR-ToF-AMS was operated during three experiments. The instrument was switched between two modalities: a single-reflectron configuration (V-mode) which offers a higher sensitivity and lower resolving power (up to ~ 2100 at *m/z* 200) and a double-reflectron configuration (W-mode) which provides a higher resolving power (up to ~ 4300 at *m/z* 200) but a lower sensitivity (De Carlo et al., 2006). Data were taken with a time resolution of 8 min. In V-mode, data were collected in the mass spectrum (MS) mode for 5 min, for aerosol quantification, and in the particle time of flight (PToF) mode for 1 min for size distribution measurement (De Carlo et al., 2006; Canagaratna et al. 2007). Only MS data were recorded in the W-mode (2 min).

The AMS data were analyzed using Squirrel (ToF-AMS Analysis 1.51B) and Pika (ToF-AMS HR Analysis 1.10B) packages for the software Igor Pro 6.21 (Wavemetrics, Inc., Portland, OR, USA). Default Collection Efficiencies (CE) and Relative Ionisation Efficiencies (RIE) were used for quantification of SOA. Air interferences were removed by adjusting the fragmentation table (Aiken et al., 2008; Allan et al., 2004). High-resolution analysis (De Carlo et al., 2006) was performed on V-mode data by integrating each CxHyOzion in the mass range 12–180 *m/z* while W-mode data were used

[Title Page](#)[Abstract](#)[Introduction](#)[Conclusions](#)[References](#)[Tables](#)[Figures](#)[|◀](#)[▶|](#)[Back](#)[Close](#)[Full Screen / Esc](#)[Printer-friendly Version](#)[Interactive Discussion](#)

only to check for possible interferences. Elemental ratios (O : C and H : C) were calculated according to the procedure described by Aiken et al. (2007, 2008). Measurement uncertainties were estimated to be ± 30 .

Further chemical analyses were performed by collecting SOA on PTFE filters (Zefluor, 47 mm diameter, 2 μm pore size, Pall Life Sciences) cut to the size of the collector using ceramic scissors. A stainless-steel support was used for sampling and concentrating the particles in a small filter area (0.9 mm^2). An active charcoal denuder was installed upstream of the filter to remove ozone and gaseous organics. Before the sampling, filters were extracted three times for 10 min with dichloromethane (99.8 %, HPLC grade) in an ultrasonic bath and baked for 5 h at 250 °C. The filter sampling was performed at a nominal flow rate of 2 L min^{-1} for a sampling time varying between 30 min to 2 h, depending on the total volume concentration of SOA in the chamber.

X-ray photoelectron spectrometry (XPS) was used to quantify the O : C ratio of the SOA surface to a depth less than 10 nm. Measurements were performed on a VG ESCALAB 250 instrument using monochromatic Al K α radiation (1486.6 eV). The X-Ray spot size was 500 μm . The analysis chamber of the instrument was maintained at pressures ranging between 10^{-8} and 10^{-11} mbar. Survey spectra of SOA were measured over an 1100 eV range at a resolution of 1 eV per step and 100 eV pass energy (Fig. S1a). All peaks were referred to the C_{1s} binding energy at 285.0 eV. The high-resolution C_{1s} spectrum showed the presence of C, O and F (Fig. S1a of the Supplement). The deconvolution of the C_{1s} signal was performed in peaks corresponding to the -CO₂ (indicative of carboxylic acids, peroxides), C-O (alcohols, aldehydes, carboxylic acids, peroxides, ethers), C-C/C-H (aliphatic functional group) and the C-F bonds of the PTFE filter in order to optimise the fit (Fig. S1b). The quantification of the O : C ratio was performed using the integrated peak areas of O_{1s} spectra, the peaks area of the -CO₂, C-O and C-C/C-H from the C_{1s} spectra and the manufacturer's sensitivity factors.

Relating hygroscopicity and optical properties

C. Denjean et al.

Title Page

Abstract

Introduction

Conclusions

References

Tables

Figures

◀

▶

◀

▶

Back

Close

Full Screen / Esc

Printer-friendly Version

Interactive Discussion



2.5 Experimental protocol

Experiments were carried out without any seed particles or an OH radical scavenger. Prior to each experiment, the CESAM chamber was evacuated to typically 4×10^{-4} mbar overnight. The chamber was then filled to atmospheric pressure with a mixture of 200 mbar of Oxygen (Air Liquide, Alphagaz class 1, purity 99.9 %) and 800 mbar of Nitrogen produced from the evaporation of a pressurised liquid nitrogen tank (Messer, purity > 99.995 %, $\text{H}_2\text{O} < 5$ ppm). Table 1 shows the experimental conditions of this study. Ozone was generated by a Corona discharge in pure O_2 using a commercial dielectric ozone generator (MBT 802N, Messtechnik GmbH, Stahnsdorf, Germany). After ozone concentration stabilisation around 250 ppb, approximately 200 ppb of α -pinene (Aldrich, 98 %) was introduced into the chamber by evaporation at a known pressure in a glass bulb of a known volume and flushing it into the chamber with a flow of oxygen. Particles were formed immediately. During the experiments, RH was lower than 1 % and the temperature ranged between 14 °C and 27 °C (for different experiments).

The physical, chemical, optical and hygroscopic properties (as measured with the H-TDMA) of SOA were monitored under dry conditions ($\text{RH} < 1$ %) for 20 h. During all the experiments, the total pressure was constantly maintained by adding gaseous nitrogen to compensate for the decrease of the pressure due to sampling by the instruments. As a consequence of this refill procedure, the $\text{N}_2 : \text{O}_2$ ratio increased with the reaction time. After 20 h of reaction, the hygroscopicity of polydisperse particles was investigated by injecting water vapour in the chamber. The RH in the chamber increased linearly from 0 to 100 % within approximately 1 h. The nephelometer was used to follow in-situ the variation in σ_{scat} as a function of RH.

Title Page	
Abstract	Introduction
Conclusions	References
Tables	Figures
	
	
Back	Close
Full Screen / Esc	
Printer-friendly Version	
Interactive Discussion	

3 Result

3.1 Reaction profile and aerosol yield

Typical evolution of α -pinene, ozone, particle number size distribution and mass concentration are shown in Fig. 2. α -pinene was essentially consumed after 4 h of reaction.

- 5 Since no OH scavenger was used, α -pinene was oxidised by O_3 and also by OH radicals produced by the reaction. A rapid formation of SOA was observed as the α -pinene was oxidised. The aerosol mass reached its maximum of $130 \pm 39 \mu\text{g m}^{-3}$ (when most α -pinene was consumed) and remained constant thereafter.

Table 1 summarises the results for the experiments conducted. The aerosol yield (Y)
10 was given by Eq. (6):

$$Y = \frac{\Delta[\text{SOA}]}{\Delta[\alpha\text{-pinene}]} \quad (6)$$

where $\Delta[\text{SOA}]$ is the SOA mass concentration produced for a given amount of α -pinene reacted, $\Delta[\alpha\text{-pinene}]$, both corrected for dilution. Since α -pinene was introduced after

15 ozone into the chamber, its initial concentration could not be directly measured. For the yield calculations, we used the SOA mass concentration and α -pinene concentration after 5 min of reaction as initial concentrations. SOA mass concentration was calculated from the SMPS number size distribution corrected for dilution and the measured particle density, assuming homogeneous spherical particles. The SOA density of 1.2 g m^{-3}

20 was estimated from the mobility mode and aerodynamic mode obtained from the SMPS and AMS measurements respectively, as described by DeCarlo et al. (2004) and Katrib et al. (2005). No significant change in the SOA density was found during the experiment. The retrieved value is in agreement with previous laboratory studies (Shilling et al., 2008; Saathoff et al., 2009). From Table 1, it can be observed that the mass

25 concentration of SOA varies from 44 to $139 \mu\text{g m}^{-3}$, resulting in calculated yields values ranging between 0.07 and 0.21 . The steady-state aerosol yields determined in this study are compared to the values reported in the literature in Fig. S2 (Supplement).

Title Page

Abstract

Introduction

Conclusions

References

Tables

Figures

◀

▶

◀

▶

Back

Close

Full Screen / Esc

Printer-friendly Version

Interactive Discussion



To facilitate the comparison with the literature, we adjusted our yield data to a SOA density of 1.0 g m^{-3} . Our yields are in agreement with Hoffmann et al. (1997), but up to 2 times lower compared to other studies. These differences are arise from instrumental and treatment uncertainties, as shown by the error bars. Shilling et al. (2008) investigated several possible artefacts and sources of error that could reasonably influence yield values. They suggested that different gas-phase chemistry or partitioning of species on the surface of the walls could occur within the chambers. However, our yields can be directly compared to the values reported by Wang et al. (2011) who performed experiments in a similar simulation chamber as ours. Our values are systematically lower than those reported by Wang et al. (2011) by approximately 20 %. One major issue differentiating our experimental conditions is the initial concentration of ozone. Wang et al. (2011) performed experiments with an excess of ozone, while we used significantly lower ozone concentration to generate SOA. It is expected that a lower concentration of OH radicals was produced from our experiments during the ozonolysis of α -pinene, which could reduce the aerosol yield of the reaction.

3.2 Complex refractive index

The real and imaginary parts of the CRI were retrieved to describe the scattering and absorbing characteristics of SOA.

The imaginary part of the CRI was estimated from the attenuation measurements obtained with the aethalometer. Since the attenuation coefficient depends on the quantity of particles accumulated on the filter, the CRI could not be calculated during the SOA formation, while the mass concentration increased rapidly until the α -pinene was consumed. Figure 3 shows that the absorption coefficient in the 370–950 nm wavelength range estimated after 14 h of reaction is close to or below zero, indicating that the SOA does not absorb radiation in the visible to near-UV region. Therefore, the imaginary part of the CRI was set to zero. This result is consistent with previous studies on the absorbing properties of α -pinene- O_3 SOA. Cappa et al. (2008) observed no significant absorption of α -pinene- O_3 SOA at 532 nm with a photoacoustic spectrometer.

[Title Page](#)[Abstract](#)[Introduction](#)[Conclusions](#)[References](#)[Tables](#)[Figures](#)[|◀](#)[▶|](#)[◀](#)[▶](#)[Back](#)[Close](#)[Full Screen / Esc](#)[Printer-friendly Version](#)[Interactive Discussion](#)

Schnaiter et al. (2003) and Nakayama et al. (2010) measured no significant differences between scattering and extinction coefficient in the visible spectrum. Nakayama et al. (2012) showed that the imaginary part of the CRI values was negligible (< 0.003) in the 405–781 nm wavelenghts. Recently, Liu et al. (2013) reported also an imaginary part of the CRI below 10^{-4} for 355 to 781 nm wavelenghts.

Figure 4a shows the real part of the retrieved CRI at 525 nm as a function of reaction time. Real CRI were calculated when SOA exhibited a diameter high enough to allow the detection of the full size distribution by the SMPS. Based on the measurement uncertainties of $\pm 10\%$ for σ_{scatt} , we estimate an absolute error associated with the real CRI of ± 0.02 . The real CRI decreased from 1.43–1.60 at the beginning of the reaction to 1.32–1.38 after 14 h of reaction. In contrast, no significant changes in the CRI were observed during the first hour of reaction for experiments E050210 and E080210. As shown in Fig. 4b, the aerosol mass concentrations in these experiments stabilised after 20 min of reaction which was significantly faster than in the other experiments. This may result from differences in the [VOC]/[O₃] concentrations (see discussion in Sect. 3.1. on the initial concentrations of α -pinene), leading to different reaction kinetics (Chan et al., 2007). The real CRI appears to change significantly in most of the experiments between 10 min and 1 h of reaction and it is possible that these variations were not detected in experiments E050210 and E080210. Values for the real part of the CRI retrieved in this study at 525 nm are compared with the literature values obtained for SOA produced during α -pinene + O₃ SOA formation (Table 2). Because experiments are performed under various time scales reaction and under various conditions and because CRI evolves with SOA ageing, we can only observe that our values (1.32–1.60) are in the same range as the previous ones.

25 3.3 Hygroscopic properties

A first insight in the hygroscopic behaviour of SOA was brought by HTDMA humidiograms. SOA in suspension in CESAM under dry condition were sampled and driven to the HTDMA. Particles of 115 nm diameter were selected for the analysis after 2 h

[Title Page](#)[Abstract](#)[Introduction](#)[Conclusions](#)[References](#)[Tables](#)[Figures](#)[|◀](#)[▶|](#)[◀](#)[▶](#)[Back](#)[Close](#)[Full Screen / Esc](#)[Printer-friendly Version](#)[Interactive Discussion](#)

ageing and 190 nm after 16 h ageing. The GF uncertainty was estimated from the uncertainty in retrieving the geometric diameters and the RH uncertainty was based on the RH sensors uncertainties at the entrance of the H-TDMA. The GF values at 90 % RH of SOA are reported in Fig. 5 as a function of time. GF ranged from 1.02 (± 0.02) to 1.07 (± 0.02) at $90 \pm 4.2\%$ RH during and after SOA formation, in agreement with values previously reported in the literature (Table 3). SOA remained hydrophobic with no variation in water uptake throughout the experiment.

The comparison of the mobility diameter as a function of RH after 2 and 16 h of SOA ageing is shown in Fig. 6. Unusual behaviour of the mobility diameter and $f(\text{RH})$ at the end of the experiment (at $t = 16\text{--}20\text{ h}$) is evident. Mobility diameters dropped to a minimum between 20–50 % RH for SOA after 16 h reaction that was not observed for “fresh” SOA. Figure 7 shows the RH dependence of $f(\text{RH})$ of the polydisperse size distribution as measured directly in the chamber after water injection during the last 1 h and 16–20 h of the experiment. Two RH scales are used: one for the measurements performed within the chamber and the other for the measurements performed using the nephelometer. In fact, a small drying of 10 % has been observed between the chamber and the nephelometer. There is a first increase of $f(\text{RH})$ as RH increases from 0 to 30 % RH. This can be due to a change in the physical state of SOA. In fact, particles with irregular shape or porous should appear at higher mobility diameter with the DMA than spherical and compact particles with the same mass (De Carlo et al., 2004). After uptake of water, SOA may become more spherical or compact, leading to a shift of the mobile size distribution measured with the DMA (Mikhailov et al., 2009). Particles are expected to exhibit also a higher mass concentration, and the σ_{scatt} should increase after humidification (Adachi et al., 2011). This hypothesis will be discussed in detail in the Sect. 4.2. A second slope is observed between 80 and 90 % RH, linked to the sharp increase of GF due to particle water absorption. All the experiments exhibited the same trend, but different values are observed at 90 % RH. This can be explained by the different size distribution from one experiment to another. In particular, the proportion

Relating hygroscopicity and optical properties

C. Denjean et al.

[Title Page](#)

[Abstract](#)

[Introduction](#)

[Conclusions](#)

[References](#)

[Tables](#)

[Figures](#)

◀

▶

[Back](#)

[Close](#)

[Full Screen / Esc](#)

[Printer-friendly Version](#)

[Interactive Discussion](#)



of particles larger than 100 nm is different resulting in a changing capacity in absorbing water (Biskos et al., 2006) and hence varying the observed $f(\text{RH})$.

3.4 Chemical composition

3.4.1 SOA chemical structure

- 5 The O : C ratio of the bulk aerosol measured online by the AMS and the O : C ratio at the surface obtained by XPS analysis on filter samples are shown in Fig. 8. The bulk O : C ratio ranged between 0.68 (± 0.20) to 0.55 (± 0.16). Bulk O : C ratio obtained in the literature from different techniques are shown in Table 4. The bulk O : C ratios retrieved in our study are in agreement with Shilling et al. (2008), Chhabra et al. (2010), Reinhardt et al. (2007) and Tolocka et al. (2006). Values at the beginning of the reaction are, 10 however, higher than those obtained by Aiken et al. (2007) and Qi et al. (2012) who used AMS to retrieve the O : C ratio. Limited information is given by Aiken et al. (2007) about their experimental conditions. In particular, temperature and time scale of reaction are critical parameters which can significantly affect the chemical composition of 15 SOA (Warren et al., 2009; Shilling et al., 2008; Chhabra et al., 2010). Qi et al. (2012) did not provide any uncertainty in their AMS measurements, but taking into account the uncertainties of $\pm 30\%$ given by Aiken et al. (2007), their O : C ratios are in agreement with our values.

- The surface O : C ratio is significantly lower and ranges between 0.33 (± 0.07) and 20 0.46 (± 0.08). This suggests that the SOA composition is not homogeneous, but composed of less oxidised species at its surface. To our knowledge, our study is the first to investigate the surface O : C ratio of the SOA and thus no comparison with literature is possible. Nevertheless, this observation is in very good agreement with one of the hypotheses by McIntire et al. (2010). The authors proposed a hydrophobic shell model 25 for hydrocarbon + O_3 SOA due to the burying of R-COOH and other polar groups inside the particle. Here, we report direct measurements which support this hypothesis.

Title Page	
Abstract	Introduction
Conclusions	References
Tables	Figures
◀	▶
◀	▶
Back	Close
Full Screen / Esc	
Printer-friendly Version	
Interactive Discussion	



3.4.2 Evolution of the SOA chemical composition

The bulk O:C ratio decreased from 0.68 (± 0.20) at the beginning of the reaction to 0.55 (± 0.16) after 9 h of reaction and remained constant until 20 h of reaction (Fig. 8). The comparison of the fraction f_{44} and f_{43} fragments provides some insights on the evolution of the SOA functionality during the reaction (Fig. 9). The fraction f_{44} is mostly representative of the organic acids (-COOH) in the AMS source (Ng et al., 2010) and can also be affected by hydroperoxide species (Sato et al., 2012). The fraction f_{43} can be linked to non-acid oxygenated species and is assumed to be dominated by the $C_2H_3O^+$ fragment (Ng et al., 2010). At the beginning of the reaction, the SOA exhibited a high value of f_{44} which decreased with reaction time. Two potential processes affecting the bulk O:C ratio and f_{44} during the SOA formation are the gas/particle phase partitioning and chemical reactions in the condensed phase. The decrease of these parameters can be explained by an increasing partitioning of less oxidised semi-volatile compounds as the aerosol grows according to the structure-activity correlation between the oxygenated functional groups and the species vapour pressure (Pankow and Asher, 2008). Additionally, some oligomerisation/dehydration, such as aldol condensation or ester formation, can alter the SOA O:C ratio and f_{44} (Camredon et al., 2010; Ziemann and Atkinson, 2012). After the consumption of the precursors, f_{44} remained constant, which can be explained by the molecular structure of α -pinene, which contains only one double bond and thus one active site for ozone reaction, limiting the gas-phase oxidation of first-generation products. Additional reactions in the particle phase can take place after the SOA formation, and can for example lead to the formation of oligomers (Kalberer et al., 2004; Gao et al., 2004a, b; Tolocka et al., 2004; Yasmeen et al., 2012; Reinhardt et al., 2007; Rudich et al., 2007), but do not appear to be associated with a significant change in the SOA functionality.

The correlation between f_{44} and f_{43} for α -pinene- O_3 SOA has also been compared to laboratory data obtained by Shilling et al. (2009) and ambient SOA ground and flight data from different sites, including Mexico city (Ng et al., 2010). Our data are within

Relating hygroscopicity and optical properties

C. Denjean et al.

Title Page

Abstract

Introduction

Conclusions

References

Tables

Figures



Back

Close

Full Screen / Esc

[Printer-friendly Version](#)

Interactive Discussion



the triangular region of the typical ambient SOA, but exhibit higher f_{44} than Shilling et al. (2009). This discrepancy may be due to the use of OH scavengers by the latter. Previous laboratory studies have observed an increase of the O : C ratio of α -pinene-O₃ SOA after OH exposure (Tritscher et al., 2011; Cappa et al., 2011; Qi et al., 2012; George and Abbatt, 2010; Donahue et al., 2012). Since f_{44} is the major contributor to the oxygen signal in the SOA spectra, this fragment may increase with OH exposure formation of carboxylic acids (Muller et al., 2012).

4 Discussion

4.1 Dependence of the CRI and GF on the chemical composition

- 10 Our results suggest that the real part CRI is closely related to SOA chemical composition. Figure 10 shows that the real part of the CRI decreases substantially as the O : C ratio of the bulk SOA decreases. This trend is in agreement with the positive correlation between the extinction coefficient at 532 nm wavelength and O : C ratio observed by Cappa et al. (2011) for the heterogeneous OH oxidation of squalane and azelaic acid
15 particles. Nakayama et al. (2013) reported increasing real part of the CRI at 532 nm with increasing O : C ratio for SOA generated from the photooxidation of toluene. Recently, Flores et al. (2014) showed that the real part of CRI at 405 nm is positively correlated to the O : C ratio for a mixture of biogenic VOC (α -pinene and limonene) and biogenic VOC mixture with subsequent addition of an anthropogenic VOC (*p*-xylene-d₁₀). On the other hand, an opposite trend was observed by Nakayama et al. (2012)
20 with a decrease of the real part of the CRI at 532 nm wavelength with increasing O : C ratio for SOA produced from the ozonolysis and photooxidation of α -pinene. Lambe et al. (2013) studied SOA formed by OH oxidation of various gas-phase precursors (naphthalene, tricyclo[5.2.1.0^{2,6}]decane, guaiacol and α -pinene) and retrieved a decreasing real part of CRI with increasing oxidation. These differences provide evidence
25

Title Page	
Abstract	Introduction
Conclusions	References
Tables	Figures
◀	▶
◀	▶
Back	Close
Full Screen / Esc	
Printer-friendly Version	
Interactive Discussion	



Relating hygroscopicity and optical properties

C. Denjean et al.

that the change of the real CRI as a function of O:C ratio depends strongly on the organic aerosol source and ageing in the atmosphere.

The decrease of bulk O : C ratio is expected to induce a decrease in SOA hygroscopic properties (Massoli et al., 2010; Jimenez et al., 2009; Chang et al., 2010; Duplissy et al., 2011). However, the GF remained surprisingly constant over 20 h of reaction. This trend contradicts with Saathoff et al. (2003) and Cocker et al. (2001) who reported an increase of the GF from 1.080 to 1.106 and 1.065 to 1.1 respectively within time scale of 6 h. However, our constant GF is consistent with the constant hygroscopicity observed by Warren et al. (2009) and Qi (2010) for α -pinene- O_3 SOA. The constant GF measured in our study may result from: (1) the sensitivity of the instruments. The GF was studied after 2 h of reaction when the decrease of the oxidation degree was slow. The O : C of bulk SOA decreased from 0.65 to 0.60 between 2 and 10 h ageing (Fig. 10), that should result in a GF decrease of 0.03 according to the linear GF-to-O : C relationship reported by Massoli et al. (2010). The variation of GF due to the chemical composition change may not be detected due to the sensitivity of the H-TDMA. (2) The core-shell structure of the SOA with less oxygenated and less hydrophilic compounds at the surface. The O : C ratio of the particle surface was significantly lower than the bulk O : C and remained constant over time (see Sect. 3.4.1.). This structure would affect the heterogeneous chemistry of the particle and avoid the water adsorption on particles. Broekhuizen et al. (2004) observed that the oxidation of oleic acid by low concentration of ozone, shown to produce oxygenated products (Moise and Rudich, 2002), did not increase the particle CCN activity. Katrib et al. (2004) demonstrated that hydrophobic products were formed at the surface of oleic acid after ozone exposure that avoided water adsorption on particles. McIntire et al. (2010) exposed particles formed from ozonolysis of surface-bound alkenes to ozone and observed formation of polar groups buried inside a hydrophobic shell. This is also consistent with Moussa et al. (2009) who observed that the uptake of water does not increase after the oxidation of surface-bound alkenes. A core–shell structure could explain the low O : C

Title Page

Abstract

Introduction

Conclusions

References

Tables

Figures



Back

Close

Full Screen / Esc

[Printer-friendly Version](#)

Interactive Discussion



ratio of the surface α -pinene-O₃ SOA obtained in the present study and could affect significantly the heterogeneous chemistry of the particle.

4.2 Effect of RH and ageing on the viscosity of SOA

An unexpected effect of ageing on the dynamic of the size distribution evolution during humidification has been observed (Sect. 3.3). For the 16 h old SOA, humidification led to a decay of the mobility diameter while such behaviour was not observed for the 2 h old SOA. As it is difficult to believe that a RH increase would induce a sudden loss of matter for the particulate phase, it is hypothesised that the particles experienced a rapid change of shape when humidified. This explanation is also in agreement with the increase of σ_{scatt} for aged SOA when the RH was increased in the chamber. Being observed for aged SOA only, these behaviours support a re-shaping of coagulated particles and increase in sphericity when relative humidity is above 20–30 %. This implies that, below this RH value, coagulated particles were not spherical and hence that they were not liquid enough to fully merge into single spheres. However, Pajunoja et al. (2014) recently analyzed SOA particles from ozonolysis of α -pinene under dry conditions (RH < 20 %) using scanning electron microscopy (SEM) and observed only spherical particles following coagulation.

A few recent studies have suggested that α -pinene-O₃ SOA is likely to be in an amorphous semi-solid or amorphous solid (glassy) state under dry conditions (RH < 30 %). Virtanen et al. (2011) reported that α -pinene-O₃ SOA bounces off impactor plates as if particles were glassy. Other studies reported that the evaporation kinetics of α -pinene-O₃ SOA was lower than expected by models for liquid droplets, indicating a nonliquid-like state (Cappa and Wilson, 2011; Vaden et al., 2011). These findings are in agreement with Perraud et al. (2012) who has shown that the uptake of organic nitrates by α -pinene-O₃ SOA did not follow absorptive equilibrium partitioning theory, as indicative of nonliquid-like behaviour. Moreover, some recent studies reported viscosity changes of α -pinene-O₃ SOA with RH. Saukko et al. (2012) observed lower bounce behaviour after the SOA was exposed to RH > 50 %, indicating a liquid-like, less viscous phase.

Title Page

Abstract

Introduction

Conclusions

References

Tables

Figures

|◀

▶|

◀

▶|

Back

Close

Full Screen / Esc

Printer-friendly Version

Interactive Discussion



Relating hygroscopicity and optical properties

C. Denjean et al.

[Title Page](#)

[Abstract](#)

[Introduction](#)

[Conclusions](#)

[References](#)

[Tables](#)

[Figures](#)

◀

▶

[Back](#)

[Close](#)

[Full Screen / Esc](#)

[Printer-friendly Version](#)

[Interactive Discussion](#)



5 Atmospheric implication and conclusion

The imaginary part of the CRI values for α -pinene-O₃ SOA was found to be negligible in the visible spectrum, indicating that these particles have a pure scattering effect. The single scattering albedo w_0 , a key parameter to estimate the influence of aerosols on the radiative balance, is estimated to be equal to 1, indicating that these particles have a cooling effect on the climate. α -pinene-O₃ SOA do not have a direct aerosol heating potential.

In order to estimate the evolution of the direct radiative effect of SOA, we calculated the mass extinction efficiency k_{ext} (dry) at 525 nm of dry SOA as the ratio of the measured σ_{scat} to the SOA mass concentration. k_{ext} depends on the competitive effect of aerosol size and chemical composition. The decrease of the real CRI resulting from the changing particle chemical composition is expected to decrease k_{ext} while the size increase of the SOA from nucleation to accumulation mode should increase k_{ext} . We obtained $k_{\text{ext}}(\text{dry}) = 0.64 \pm 0.27 \text{ m}^2 \text{ g}^{-1}$ at the beginning of the SOA formation, that is significantly lower than the value of $k_{\text{ext}}(\text{dry}) = 1.68 \pm 0.50 \text{ m}^2 \text{ g}^{-1}$ obtained after 14 h reaction.

The mass extinction efficiency k_{ext} is also strongly affected by the ambient relative humidity. α -pinene-O₃ SOA did not show deliquescence below 90 % RH, but a continuous water uptake with increasing RH. A constant GF (90 % RH) was obtained throughout the experiment. From the measured $f(90 \% \text{ RH})$ and GF(90 % RH) obtained in this study, we can estimate σ_{scat} and SOA mass concentration at 90 % RH and then $k_{\text{ext}}(90 \% \text{ RH}) = 2.36 \pm 0.70 \text{ m}^2 \text{ g}^{-1}$. Water uptake by SOA at 90 % RH produces an increase of k_{ext} by 40 %. This simple calculation highlights the importance of taking into account the actual ambient conditions that the α -pinene-O₃ SOA experiences during its lifetime when estimating its induced direct radiative effect in the atmosphere.

Relating hygroscopicity and optical properties

C. Denjean et al.

[Title Page](#)

[Abstract](#)

[Introduction](#)

[Conclusions](#)

[References](#)

[Tables](#)

[Figures](#)

◀

▶

◀

▶

[Back](#)

[Close](#)

[Full Screen / Esc](#)

[Printer-friendly Version](#)

[Interactive Discussion](#)



Acknowledgements. This research work has been supported by the European Community within the seventh Framework Programme: Eurochamp-2 (EU-FP7 grant agreement no. 228335). We also acknowledge the National Research Agency ANR (project Cumulus). We thank Frank Siekmann and Sylvain Ravier (Aix-Marseille Université, France) for their help in calibrating the AMS during the measurement campaign. We thank Brendan Mahon and Steven J. Campbell (University of Cambridge, UK) for helpful revision of the manuscript.

References

- Abramson, E., Imre, D., Beranek, J., Wilson, J., and Zelenyuk, A.: Experimental determination of chemical diffusion within secondary organic aerosol particles, *Phys. Chem. Chem. Phys.*, 15, 2983–2991, doi:10.1039/C2CP44013J, 2013.
- Adachi, K., Freney, E. J., and Buseck, P. R.: Shapes of internally mixed hygroscopic aerosol particles after deliquescence, and their effect on light scattering, *Geophys. Res. Lett.*, 38, L13804, doi:10.1029/2011GL047540, 2011.
- Aiken, A. C., DeCarlo, P. F., and Jimenez, J. L.: Elemental analysis of organic species with electron ionization high-resolution mass spectrometry, *Anal. Chem.*, 79, 8350–8358, 2007.
- Aiken, A. C., DeCarlo, P. F., Kroll, J. H., Worsnop, D. R., Huffman, J. A., Docherty, K. S., Ulbrich, I. M., Mohr, C., Kimmel, J. R., Sueper, D., Sun, Y., Zhang, Q., Trimborn, A., Northway, M., Ziemann, P. J., Canagaratna, M. R., Onasch, T. B., Alfarra, M. R., Prevot, A. S. H., Dommen, J., Duplissy, J., Metzger, A., Baltensperger, U., and Jimenez, J. L.: O/C and OM/OC ratios of primary, secondary, and ambient organic aerosols with high-resolution time-of-flight aerosol mass spectrometry, *Environ. Sci. Technol.*, 42, 4478–4485, doi:10.1021/es703009q, 2008.
- Allan, J. D., Delia, A. E., Coe, H., Bower, K. N., Alfarra, M. R., Jimenez, J. L., Middlebrook, A. M., Drewnick, F., Onasch, T. B., Canagaratna, M. R., Jayne, J. T., and Worsnop, D. R.: A generalised method for the extraction of chemically resolved mass spectra from aerodynamic aerosol

Title Page

Abstract

Introduction

Conclusions

References

Tables

Figures

◀

▶

◀

▶

Back

Close

Full Screen / Esc

Printer-friendly Version

Interactive Discussion



Relating hygroscopicity and optical properties

C. Denjean et al.

[Title Page](#)

[Abstract](#)

[Introduction](#)

[Conclusions](#)

[References](#)

[Tables](#)

[Figures](#)

◀

▶

[Back](#)

[Close](#)

[Full Screen / Esc](#)

[Printer-friendly Version](#)

[Interactive Discussion](#)



- Cappa, C. D. and Wilson, K. R.: Evolution of organic aerosol mass spectra upon heating: implications for OA phase and partitioning behavior, *Atmos. Chem. Phys.*, 11, 1895–1911, doi:10.5194/acp-11-1895-2011, 2011.
- 5 Cappa, C. D., Lack, D. A., Burkholder, J. B., and Ravishankara, A. R.: Bias in filter-based aerosol light absorption measurements due to organic aerosol loading: evidence from laboratory measurements, *Aerosol Sci. Tech.*, 42, 1022–1032, 2008.
- Cappa, C. D., Che, D. L., Kessler, S. H., Kroll, J. H., and Wilson, K. R.: Variations in organic aerosol optical and hygroscopic properties upon heterogeneous OH oxidation, *J. Geophys. Res.*, 116, D15204, doi:10.1029/2011JD015918, 2011.
- 10 Carrico, C. M., Kreidenweis, S. M., Malm, W. C., Day, D. E., Lee, T., Carrillo, J., McMeeking, G. R., and Collett Jr., J. L.: Hygroscopic growth behavior of a carbon-dominated aerosol in Yosemite National Park, *Atmos. Environ.*, 39, 1393–1404, 2005.
- 15 Chan, A. W. H., Kroll, J. H., Ng, N. L., and Seinfeld, J. H.: Kinetic modeling of secondary organic aerosol formation: effects of particle- and gas-phase reactions of semivolatile products, *Atmos. Chem. Phys.*, 7, 4135–4147, doi:10.5194/acp-7-4135-2007, 2007.
- 20 Chang, R. Y.-W., Slowik, J. G., Shantz, N. C., Vlasenko, A., Liggio, J., Sjostedt, S. J., Leaitch, W. R., and Abbatt, J. P. D.: The hygroscopicity parameter (κ) of ambient organic aerosol at a field site subject to biogenic and anthropogenic influences: relationship to degree of aerosol oxidation, *Atmos. Chem. Phys.*, 10, 5047–5064, doi:10.5194/acp-10-5047-2010, 2010.
- 25 Charlson, R. J., Schwartz, S. E., Hales, J. M., Cess, R. D., Coakley, J. A., Hansen, J. E., and Hofmann, D. J.: Climate forcing by anthropogenic aerosols, *Science*, 255, 423–430, doi:10.1126/science.255.5043.423, 1992.
- 30 Chen, Q., Liu, Y. J., Donahue, N. M., Shilling, J. E., and Martin, S. T.: Particle-phase chemistry of secondary organic material: modeled compared to measured O : C and H : C elemental ratios provide constraints, *Environ. Sci. Technol.*, 45, 4763–4770, doi:10.1021/es104398s, 2011.
- Chhabra, P. S., Flagan, R. C., and Seinfeld, J. H.: Elemental analysis of chamber organic aerosol using an aerodyne high-resolution aerosol mass spectrometer, *Atmos. Chem. Phys.*, 10, 4111–4131, doi:10.5194/acp-10-4111-2010, 2010.
- 35 Chung, S. H. and Seinfeld, J. H.: Global distribution and climate forcing of carbonaceous aerosols, *J. Geophys. Res.*, 107, 4407, doi:10.1029/2001JD001397, 2002.

[Title Page](#)[Abstract](#)[Introduction](#)[Conclusions](#)[References](#)[Tables](#)[Figures](#)[◀](#)[▶](#)[◀](#)[▶](#)[Back](#)[Close](#)[Full Screen / Esc](#)[Printer-friendly Version](#)[Interactive Discussion](#)

Cocker, D. R., Mader, B. T., Kalberer, M., Flagan, R. C., and Seinfeld, J. H.: The effect of water on gas-particle partitioning of secondary organic aerosol: II. M-xylene and 1,3,5-trimethylbenzene photooxidation systems, *Atmos. Environ.*, 35, 6073–6085, doi:10.1016/s1352-2310(01)00405-8, 2001.

- 5 Collaud Coen, M., Weingartner, E., Apituley, A., Ceburnis, D., Fierz-Schmidhauser, R., Flentje, H., Henzing, J. S., Jennings, S. G., Moerman, M., Petzold, A., Schmid, O., and Baltensperger, U.: Minimizing light absorption measurement artifacts of the Aethalometer: evaluation of five correction algorithms, *Atmos. Meas. Tech.*, 3, 457–474, doi:10.5194/amt-3-457-2010, 2010.
- 10 DeCarlo, P. F., Kimmel, J. R., Trimborn, A., Northway, M. J., Jayne, J. T., Aiken, A. C., Gonin, M., Fuhrer, K., Horvath, T., Docherty, K. S., Worsnop, D. R., and Jimenez, J. L.: Field-deployable, high-resolution, time-of-flight aerosol mass spectrometer, *Anal. Chem.*, 78, 8281–8289, doi:10.1021/ac061249n, 2006.
- 15 de Gouw, J. A., Middlebrook, A. M., Warneke, C., Goldan, P. D., Kuster, W. C., Roberts, J. M., Fehsenfeld, F. C., Worsnop, D. R., Canagaratna, M. R., Pszenny, A. A. P., Keene, W. C., Marchewka, M., Bertman, S. B., and Bates, T. S.: Budget of organic carbon in a polluted atmosphere: results from the New England Air Quality Study in 2002, *J. Geophys. Res.-Atmos.*, 110, D16305, doi:10.1029/2004jd005623, 2005.
- 20 Denjean, C., Formenti, P., Picquet-Varrault, B., Katrib, Y., Pangui, E., Zapf, P., and Doussin, J. F.: A new experimental approach to study the hygroscopic and optical properties of aerosols: application to ammonium sulfate particles, *Atmos. Meas. Tech.*, 7, 183–197, doi:10.5194/amt-7-183-2014, 2014.
- 25 Dinar, E., Riziq, A. A., Spindler, C., Erlick, C., Kiss, G., and Rudich, Y.: The complex refractive index of atmospheric and model humic-like substances (HULIS) retrieved by a cavity ring down aerosol spectrometer (CRD-AS), *Faraday Discuss.*, 137, 279–295, doi:10.1039/b703111d, 2008.
- Docherty, K. S., Wu, W., Lim, Y. B., and Ziemann, P. J.: Contributions of organic peroxides to secondary aerosol formed from reactions of monoterpenes with O₃, *Environ. Sci. Technol.*, 39, 4049–4059, doi:10.1021/es050228s, 2005.
- 30 Donahue, N. M., Henry, K. M., Mentel, T. F., Kiendler-Scharr, A., Spindler, C., Bohn, B., Brauers, T., Dorn, H. P., Fuchs, H., Tillmann, R., Wahner, A., Saathoff, H., Naumann, K. H., Mohler, O., Leisner, T., Muller, L., Reinnig, M. C., Hoffmann, T., Salo, K., Hallquist, M., Frosch, M., Bilde, M., Tritscher, T., Barmet, P., Praplan, A. P., DeCarlo, P. F., Dom-

Relating
hygroscopicity and
optical properties

C. Denjean et al.

[Title Page](#)[Abstract](#)[Introduction](#)[Conclusions](#)[References](#)[Tables](#)[Figures](#)[◀](#)[▶](#)[◀](#)[▶](#)[Back](#)[Close](#)[Full Screen / Esc](#)[Printer-friendly Version](#)[Interactive Discussion](#)

- men, J., Prevot, A. S. H., and Baltensperger, U.: Aging of biogenic secondary organic aerosol via gas-phase OH radical reactions, *P. Natl. Acad. Sci. USA*, 109, 13503–13508, doi:10.1073/pnas.1115186109, 2012.
- Duplissy, J., DeCarlo, P. F., Dommen, J., Alfarra, M. R., Metzger, A., Barmpadimos, I., Prevot, A. S. H., Weingartner, E., Tritscher, T., Gysel, M., Aiken, A. C., Jimenez, J. L., Canagaratna, M. R., Worsnop, D. R., Collins, D. R., Tomlinson, J., and Baltensperger, U.: Relating hygroscopicity and composition of organic aerosol particulate matter, *Atmos. Chem. Phys.*, 11, 1155–1165, doi:10.5194/acp-11-1155-2011, 2011.
- Dusek, U., Reischl, G. P., and Hitzenberger, R.: CCN activation of pure and coated carbon black particles, *Environ. Sci. Technol.*, 40, 1223–1230, 2006.
- Flores, J. M., Zhao, D. F., Segev, L., Schlag, P., Kiendler-Scharr, A., Fuchs, H., Watne, Å. K., Bluvshtein, N., Mentel, Th. F., Hallquist, M., and Rudich, Y.: Evolution of the complex refractive index in the near UV spectral region in ageing secondary organic aerosol, *Atmos. Chem. Phys. Discuss.*, 14, 4149–4187, doi:10.5194/acpd-14-4149-2014, 2014.
- Gao, S., Keywood, M., Ng, N. L., Surratt, J., Varutbangkul, V., Bahreini, R., Flagan, R. C., and Seinfeld, J. H.: Low-molecular-weight and oligomeric components in secondary organic aerosol from the ozonolysis of cycloalkenes and alpha-pinene, *J. Phys. Chem. A*, 108, 10147–10164, doi:10.1021/jp047466e, 2004a.
- Gao, S., Ng, N. L., Keywood, M., Varutbangkul, V., Bahreini, R., Nenes, A., He, J., Yoo, K. Y., Beauchamp, J. L., Hodyss, R. P., Flagan, R. C., and Seinfeld, J. H.: Particle phase acidity and oligomer formation in secondary organic aerosol, *Environ. Sci. Technol.*, 38, 6582–6589, 2004b.
- George, I. J. and Abbatt, J. P. D.: Chemical evolution of secondary organic aerosol from OH-initiated heterogeneous oxidation, *Atmos. Chem. Phys.*, 10, 5551–5563, doi:10.5194/acp-10-5551-2010, 2010.
- Goldstein, A. H. and Galbally, I. E.: Known and unexplored organic constituents in the Earth's atmosphere, *Geochim. Cosmochim. Ac.*, 73, A449–A449, 2009.
- Griffin, R. J., Cocker III, D. R., Seinfeld, J. H., and Dabdub, D.: Estimate of global atmospheric organic aerosol from oxidation of biogenic hydrocarbons, *Geophys. Res. Lett.*, 26, 2721–2724, 1999.
- Guenther, A., Hewitt, C. N., Erickson, D., Fall, R., Geron, C., Graedel, T., Harley, P., Klinger, L., Lerdau, M., Mckay, W. A., Pierce, T., Scholes, B., Steinbrecher, R., Tallamraju, R., Taylor, J.,

Title Page

Abstract

Introduction

Conclusions

References

Tables

Figures

◀

▶

◀

▶

Back

Close

Full Screen / Esc

Printer-friendly Version

Interactive Discussion



**Relating
hygroscopicity and
optical properties**

C. Denjean et al.

[Title Page](#)[Abstract](#)[Introduction](#)[Conclusions](#)[References](#)[Tables](#)[Figures](#)[◀](#)[▶](#)[◀](#)[▶](#)[Back](#)[Close](#)[Full Screen / Esc](#)[Printer-friendly Version](#)[Interactive Discussion](#)

Relating
hygroscopicity and
optical properties

C. Denjean et al.

Title Page

Abstract

Introduction

Conclusions

References

Tables

Figures

◀

▶

◀

▶

Back Close

Full Screen / Esc

Printer-friendly Version

Interactive Discussion



vot, A. S. H., Fisseha, R., Weingartner, E., Frankevich, V., Zenobi, R., and Baltensperger, U.: Identification of polymers as major components of atmospheric organic aerosols, *Science*, 303, 1659–1662, doi:10.1126/science.1092185, 2004.

Kanakidou, M., Seinfeld, J. H., Pandis, S. N., Barnes, I., Dentener, F. J., Facchini, M. C., Van Dingenen, R., Ervens, B., Nenes, A., Nielsen, C. J., Swietlicki, E., Putaud, J. P., Balkanski, Y., Fuzzi, S., Horth, J., Moortgat, G. K., Winterhalter, R., Myhre, C. E. L., Tsigaridis, K., Vignati, E., Stephanou, E. G., and Wilson, J.: Organic aerosol and global climate modelling: a review, *Atmos. Chem. Phys.*, 5, 1053–1123, doi:10.5194/acp-5-1053-2005, 2005.

Kannisto, J., Yli-Pirila, P., Hao, L. Q., Leskinen, J., Jokiniemi, J., Makela, J. M., Joutsensaari, J., Laaksonen, A., Worsnop, D. R., Keskinen, J., and Virtanen, A.: Bounce characteristics of α -pinene-derived SOA particles with implications to physical phase, *Boreal Environ. Res.*, 18, 329–340, 2013.

Katrib, Y., Martin, S. T., Rudich, Y., Davidovits, P., Jayne, J. T., and Worsnop, D. R.: Density changes of aerosol particles as a result of chemical reaction, *Atmos. Chem. Phys.*, 5, 275–291, doi:10.5194/acp-5-275-2005, 2005.

Kavouras, I. G., Mihalopoulos, N., and Stephanou, E. G.: Formation of atmospheric particles from organic acids produced by forests, *Nature*, 395, 683–686, 1998.

Kavouras, I. G., Mihalopoulos, N., and Stephanou, E. G.: Formation and gas/particle partitioning of monoterpenes photo-oxidation products over forests, *Geophys. Res. Lett.*, 26, 55–58, doi:10.1029/1998gl900251, 1999.

Kim, H. and Paulson, S. E.: Real refractive indices and volatility of secondary organic aerosol generated from photooxidation and ozonolysis of limonene, α -pinene and toluene, *Atmos. Chem. Phys.*, 13, 7711–7723, doi:10.5194/acp-13-7711-2013, 2013.

Kim, H., Barkey, B., and Paulson, S. E.: Real refractive indices of α - and β -pinene and toluene secondary organic aerosols generated from ozonolysis and photo-oxidation, *J. Geophys. Res.*, 115, D24212, doi:10.1029/2010JD014549, 2010.

Kinne, S., Lohmann, U., Feichter, J., Schulz, M., Timmreck, C., Ghan, S., Easter, R., Chin, M., Ginoux, P., Takemura, T., Tegen, I., Koch, D., Herzog, M., Penner, J., Pitari, G., Holben, B., Eck, T., Smirnov, A., Dubovik, O., Slutsker, I., Tanre, D., Torres, O., Mishchenko, M., Geogdzhayev, I., Chu, D. A., and Kaufman, Y.: Monthly averages of aerosol properties: a global comparison among models, satellite data, and AERONET ground data, *J. Geophys. Res.-Atmos.*, 108, 4634, doi:10.1029/2001jd001253, 2003.

- Koop, T., Bookhold, J., Shiraiwa, M., and Poschl, U.: Glass transition and phase state of organic compounds: dependency on molecular properties and implications for secondary organic aerosols in the atmosphere, *Phys. Chem. Chem. Phys.*, 13, 19238–19255, doi:10.1039/C1CP22617G, 2011.
- 5 Kroll, J. H. and Seinfeld, J. H.: Chemistry of secondary organic aerosol: formation and evolution of low-volatility organics in the atmosphere, *Atmos. Environ.*, 42, 3593–3624, doi:10.1016/j.atmosenv.2008.01.003, 2008.
- Lambe, A. T., Cappa, C. D., Massoli, P., Onasch, T. B., Forestieri, S. D., Martin, A. T., Cummings, M. J., Croasdale, D. R., Brune, W. H., Worsnop, D. R., and Davidovits, P.: Relationship between oxidation level and optical properties of secondary organic aerosol, *Environ. Sci. Technol.*, 47, 6349–6357, doi:10.1021/es401043j, 2013.
- 10 Lang-Yona, N., Rudich, Y., Mentel, Th. F., Bohne, A., Buchholz, A., Kiendler-Scharr, A., Kleist, E., Spindler, C., Tillmann, R., and Wildt, J.: The chemical and microphysical properties of secondary organic aerosols from Holm Oak emissions, *Atmos. Chem. Phys.*, 10, 7253–7265, doi:10.5194/acp-10-7253-2010, 2010.
- 15 Liu, P., Zhang, Y., and Martin, S. T.: Complex refractive indices of thin films of secondary organic materials by spectroscopic ellipsometry from 220 to 1200 nm, *Environ. Sci. Technol.*, 47, 13594–13601, doi:10.1021/es403411e, 2013.
- Liu, Y. G. and Daum, P. H.: Relationship of refractive index to mass density and self-consistency 20 of mixing rules for multicomponent mixtures like ambient aerosols, *J. Aerosol Sci.*, 39, 974–986, doi:10.1016/j.jaerosci.2008.06.006, 2008.
- Lohmann, U. and Feichter, J.: Global indirect aerosol effects: a review, *Atmos. Chem. Phys.*, 5, 715–737, doi:10.5194/acp-5-715-2005, 2005.
- Martin, S. T.: Phase transitions of aqueous atmospheric particles, *Chem. Rev.*, 100, 3403–3453, 25 doi:10.1021/cr990034t, 2000.
- Massoli, P., Lambe, A. T., Ahern, A. T., Williams, L. R., Ehn, M., Mikkil*, J., Canagaratna, M. R., Brune, W. H., Onasch, T. B., Jayne, J. T., Petäjä, T., Kulmala, M., Laaksonen, A., Kolb, C. E., Davidovits, P., and Worsnop, D. R.: Relationship between aerosol oxidation level and hygroscopic properties of laboratory generated secondary organic aerosol (SOA) particles, *Geophys. Res. Lett.*, 37, L24801, doi:10.1029/2010GL045258, 2010.
- 30 Matsumoto, K., Tanaka, H., Nagao, I., and Ishizaka, Y.: Contribution of particulate sulfate and organic carbon to cloud condensation nuclei in the marine atmosphere, *Geophys. Res. Lett.*, 24, 655–658, doi:10.1029/97gl00541, 1997.

Title Page	Abstract	Introduction
Conclusions	References	
Tables	Figures	
◀	▶	
◀	▶	
Back	Close	
Full Screen / Esc		
	Printer-friendly Version	
	Interactive Discussion	



Relating
hygroscopicity and
optical properties

C. Denjean et al.

McFiggans, G., Artaxo, P., Baltensperger, U., Coe, H., Facchini, M. C., Feingold, G., Fuzzi, S., Gysel, M., Laaksonen, A., Lohmann, U., Mentel, T. F., Murphy, D. M., O'Dowd, C. D., Snider, J. R., and Weingartner, E.: The effect of physical and chemical aerosol properties on warm cloud droplet activation, *Atmos. Chem. Phys.*, 6, 2593–2649, doi:10.5194/acp-6-2593-2006, 2006.

McIntire, T. M., Ryder, O. S., Gassman, P. L., Zhu, Z., Ghosal, S., and Finlayson-Pitts, B. J.: Why ozonolysis may not increase the hydrophilicity of particles, *Atmos. Environ.*, 44, 939–944, doi:10.1016/j.atmosenv.2009.11.009, 2010.

Meyer, N. K., Duplissy, J., Gysel, M., Metzger, A., Dommen, J., Weingartner, E., Alfarra, M. R., Prevot, A. S. H., Fletcher, C., Good, N., McFiggans, G., Jonsson, Å. M., Hallquist, M., Baltensperger, U., and Ristovski, Z. D.: Analysis of the hygroscopic and volatile properties of ammonium sulphate seeded and unseeded SOA particles, *Atmos. Chem. Phys.*, 9, 721–732, doi:10.5194/acp-9-721-2009, 2009.

Mikhailov, E., Vlasenko, S., Martin, S. T., Koop, T., and Pöschl, U.: Amorphous and crystalline aerosol particles interacting with water vapor: conceptual framework and experimental evidence for restructuring, phase transitions and kinetic limitations, *Atmos. Chem. Phys.*, 9, 9491–9522, doi:10.5194/acp-9-9491-2009, 2009.

Moise, T. and Rudich, Y.: Reactive uptake of ozone by aerosol-associated unsaturated fatty acids: kinetics, mechanism, and products, *J. Phys. Chem. A*, 106, 6469–6476, doi:10.1021/jp025597e, 2002.

Moussa, S. G., McIntire, T. M., Szőri, M., Roeselová, M., Tobias, D. J., Grimm, R. L., Hemminger, J. C., and Finlayson-Pitts, B. J.: Experimental and theoretical characterization of adsorbed water on self-assembled monolayers: understanding the interaction of water with atmospherically relevant surfaces†, *J. Phys. Chem. A*, 113, 2060–2069, doi:10.1021/jp808710n, 2009.

Müller, L., Reinnig, M.-C., Naumann, K. H., Saathoff, H., Mentel, T. F., Donahue, N. M., and Hoffmann, T.: Formation of 3-methyl-1,2,3-butanetricarboxylic acid via gas phase oxidation of pinonic acid – a mass spectrometric study of SOA aging, *Atmos. Chem. Phys.*, 12, 1483–1496, doi:10.5194/acp-12-1483-2012, 2012.

Müller, T., Laborde, M., Kassell, G., and Wiedensohler, A.: Design and performance of a three-wavelength LED-based total scatter and backscatter integrating nephelometer, *Atmos. Meas. Tech.*, 4, 1291–1303, doi:10.5194/amt-4-1291-2011, 2011.

Title Page	Introduction
Abstract	References
Conclusions	Tables
Tables	Figures
◀	▶
◀	▶
Back	Close
Full Screen / Esc	
Printer-friendly Version	
Interactive Discussion	



- Murray, B. J.: Inhibition of ice crystallisation in highly viscous aqueous organic acid droplets, *Atmos. Chem. Phys.*, 8, 5423–5433, doi:10.5194/acp-8-5423-2008, 2008.
- Nakayama, T., Matsumi, Y., Sato, K., Imamura, T., Yamazaki, A., and Uchiyama, A.: Laboratory studies on optical properties of secondary organic aerosols generated during the photooxidation of toluene and the ozonolysis of alpha-pinene, *J. Geophys. Res.-Atmos.*, 115, D24204, doi:10.1029/2010jd014387, 2010.
- Nakayama, T., Sato, K., Matsumi, Y., Imamura, T., Yamazaki, A., and Uchiyama, A.: Wavelength dependence of refractive index of secondary organic aerosols generated during the ozonolysis and photooxidation of α -pinene, *Sola*, 8, 119–123, doi:10.2151/sola.2012-030, 2012.
- Nemesure, S., Wagener, R., and Schwartz, S. E.: Direct shortwave forcing of climate by the anthropogenic sulfate aerosol: sensitivity to particle size, composition, and relative humidity, *J. Geophys. Res.-Atmos.*, 100, 26105–26116, doi:10.1029/95jd02897, 1995.
- Ng, N. L., Canagaratna, M. R., Zhang, Q., Jimenez, J. L., Tian, J., Ulbrich, I. M., Kroll, J. H., Docherty, K. S., Chhabra, P. S., Bahreini, R., Murphy, S. M., Seinfeld, J. H., Hildebrandt, L., Donahue, N. M., DeCarlo, P. F., Lanz, V. A., Prévôt, A. S. H., Dinar, E., Rudich, Y., and Worsnop, D. R.: Organic aerosol components observed in Northern Hemispheric datasets from Aerosol Mass Spectrometry, *Atmos. Chem. Phys.*, 10, 4625–4641, doi:10.5194/acp-10-4625-2010, 2010.
- Novakov, T. and Penner, J. E.: Large contribution of organic aerosols to cloud-condensation nuclei, *Nature*, 365, 823–826, doi:10.1038/365823a0, 1993.
- O'Donnell, D., Tsigaridis, K., and Feichter, J.: Estimating the direct and indirect effects of secondary organic aerosols using ECHAM5-HAM, *Atmos. Chem. Phys.*, 11, 8635–8659, doi:10.5194/acp-11-8635-2011, 2011.
- Onasch, T. B., Alfarra, M. R., Williams, P. I., Bower, K., Kondo, Y., Schneider, J., Drewnick, F., Borrmann, S., Weimer, S., Demerjian, K., Salcedo, D., Cottrell, L., Griffin, R., Takami, A., Miyoshi, T., Hatakeyama, S., Shimono, A., Sun, J. Y., Zhang, Y. M., Dzepina, K., Kimmel, J. R., Sueper, D., Jayne, J. T., Herndon, S. C., Trimborn, A. M., Williams, L. R., Wood, E. C., Middlebrook, A. M., Kolb, C. E., Baltensperger, U., and Worsnop, D. R.: Evolution of organic aerosols in the atmosphere, *Science*, 326, 1525–1529, 2009.
- Orr Jr., C., Hurd, F. K., and Corbett, W. J.: Aerosol size and relative humidity, *J. Coll. Sci. Imp. U. Tok.*, 13, 472–482, doi:10.1016/0095-8522(58)90055-2, 1958.

Title Page	
Abstract	Introduction
Conclusions	References
Tables	Figures
	
	
Back	Close
Full Screen / Esc	
Printer-friendly Version	
Interactive Discussion	



Relating hygroscopicity and optical properties

C. Denjean et al.

- Pajunoja, A., Malila, J., Hao, L. Q., Joutsensaari, J., Lehtinen, K. E. J., and Virtanen, A.: Estimating the viscosity range of SOA particles based on their coalescence time, *Aerosol Sci. Tech.*, 48, I–IV, doi:10.1080/02786826.2013.870325, 2014.
- Pankow, J. F. and Asher, W. E.: SIMPOL.1: a simple group contribution method for predicting vapor pressures and enthalpies of vaporization of multifunctional organic compounds, *Atmos. Chem. Phys.*, 8, 2773–2796, doi:10.5194/acp-8-2773-2008, 2008.
- Pankow, J. F., Storey, J. M. E., and Yamasaki, H.: Effects of relative-humidity on gas-particle partitioning of semivolatile organic-compounds to urban particulate matter, *Environ. Sci. Technol.*, 27, 2220–2226, doi:10.1021/es00047a032, 1993.
- Paulson, S. E., Chung, M., Sen, A. D., and Orzechowska, G.: Measurement of OH radical formation from the reaction of ozone with several biogenic alkenes, *J. Geophys. Res.-Atmos.*, 103, 25533–25539, doi:10.1029/98jd01951, 1998.
- Pere, J. C., Mallet, M., Pont, V., and Bessagnet, B.: Impact of aerosol direct radiative forcing on the radiative budget, surface heat fluxes, and atmospheric dynamics during the heat wave of summer 2003 over western Europe: a modeling study, *J. Geophys. Res.-Atmos.*, 116, D23119, doi:10.1029/2011jd016240, 2011.
- Perraud, V., Bruns, E. A., Ezell, M. J., Johnson, S. N., Yu, Y., Alexander, M. L., Zelenyuk, A., Imre, D., Chang, W. L., Dabdub, D., Pankow, J. F., and Finlayson-Pitts, B. J.: Nonequilibrium atmospheric secondary organic aerosol formation and growth, *P. Natl. Acad. Sci. USA*, 109, 2836–2841, doi:10.1073/pnas.1119909109, 2012.
- Petters, M. D. and Kreidenweis, S. M.: A single parameter representation of hygroscopic growth and cloud condensation nucleus activity, *Atmos. Chem. Phys.*, 7, 1961–1971, doi:10.5194/acp-7-1961-2007, 2007.
- Prenni, A. J., DeMott, P. J., and Kreidenweis, S. M.: Water uptake of internally mixed particles containing ammonium sulfate and dicarboxylic acids, *Atmos. Environ.*, 37, 4243–4251, 2003.
- Qi, L.: Can secondary organic aerosol formed in an atmospheric simulation chamber continuously age?, *Atmos. Environ.*, 44, 2990–2996, 2010.
- Qi, L., Nakao, S., and Cocker, D. R.: Aging of secondary organic aerosol from α -pinene ozonolysis: roles of hydroxyl and nitrate radicals, *J. Air Waste Manage.*, 62, 1359–1369, doi:10.1080/10962247.2012.712082, 2012.
- Redmond, H. and Thompson, J. E.: Evaluation of a quantitative structure–property relationship (QSPR) for predicting mid-visible refractive index of secondary organic aerosol (SOA), *Phys. Chem. Chem. Phys.*, 13, 6872–6882, doi:10.1039/c0cp02270e, 2011.

Title Page	
Abstract	Introduction
Conclusions	References
Tables	Figures
	
	
Back	Close
Full Screen / Esc	
Printer-friendly Version	
Interactive Discussion	



- Reinhardt, A., Emmenegger, C., Gerrits, B., Panse, C., Dommen, J., Baltensperger, U., Zenobi, R., and Kalberer, M.: Ultrahigh mass resolution and accurate mass measurements as a tool to characterize oligomers in secondary organic aerosols, *Anal. Chem.*, 79, 4074–4082, doi:10.1021/ac062425v, 2007.
- 5 Renbaum-Wolff, L., Grayson, J. W., Bateman, A. P., Kuwata, M., Sellier, M., Murray, B. J., Shilling, J. E., Martin, S. T., and Bertram, A. K.: Viscosity of α -pinene secondary organic material and implications for particle growth and reactivity, *P. Natl. Acad. Sci. USA*, 110, 8014–8019, doi:10.1073/pnas.1219548110, 2013.
- RiveraCarpio, C. A., Corrigan, C. E., Novakov, T., Penner, J. E., Rogers, C. F., and Chow, J. C.:
10 Derivation of contributions of sulfate and carbonaceous aerosols to cloud condensation nuclei from mass size distributions, *J. Geophys. Res.-Atmos.*, 101, 19483–19493, doi:10.1029/95jd01077, 1996.
- Roth, C. M., Goss, K. U., and Schwarzenbach, R. P.: Sorption of a diverse set of organic vapors to urban aerosols, *Environ. Sci. Technol.*, 39, 6638–6643, doi:10.1021/es0503837, 2005.
- 15 Rudich, Y., Donahue, N. M., and Mentel, T. F.: Aging of organic aerosol: bridging the gap between laboratory and field studies, *Annu. Rev. Phys. Chem.*, Annual Reviews, Palo Alto, 321–352, 2007.
- Saathoff, H., Naumann, K.-H., Schnaiter, M., Schöck, W., Möhler, O., Schurath, U., Weingartner, E., Gysel, M., and Baltensperger, U.: Coating of soot and $(\text{NH}_4)_2\text{SO}_4$ particles by ozonolysis products of $[\alpha]$ -pinene, *J. Aerosol Sci.*, 34, 1297–1321, 2003.
- 20 Saathoff, H., Naumann, K.-H., Möhler, O., Jonsson, Å. M., Hallquist, M., Kiendler-Scharr, A., Mentel, Th. F., Tillmann, R., and Schurath, U.: Temperature dependence of yields of secondary organic aerosols from the ozonolysis of α -pinene and limonene, *Atmos. Chem. Phys.*, 9, 1551–1577, doi:10.5194/acp-9-1551-2009, 2009.
- Sato, K., Takami, A., Kato, Y., Seta, T., Fujitani, Y., Hikida, T., Shimono, A., and Imamura, T.: AMS and LC/MS analyses of SOA from the photooxidation of benzene and 1,3,5-trimethylbenzene in the presence of NO_x : effects of chemical structure on SOA aging, *Atmos. Chem. Phys.*, 12, 4667–4682, doi:10.5194/acp-12-4667-2012, 2012.
- 25 Saukko, E., Lambe, A. T., Massoli, P., Koop, T., Wright, J. P., Croasdale, D. R., Pedernera, D. A., Onasch, T. B., Laaksonen, A., Davidovits, P., Worsnop, D. R., and Virtanen, A.: Humidity-dependent phase state of SOA particles from biogenic and anthropogenic precursors, *Atmos. Chem. Phys.*, 12, 7517–7529, doi:10.5194/acp-12-7517-2012, 2012.

Relating hygroscopicity and optical properties

C. Denjean et al.

[Title Page](#)

[Abstract](#)

[Introduction](#)

[Conclusions](#)

[References](#)

[Tables](#)

[Figures](#)

◀

▶

◀

▶

[Back](#)

[Close](#)

[Full Screen / Esc](#)

[Printer-friendly Version](#)

[Interactive Discussion](#)



- Saunders, S. M., Jenkin, M. E., Derwent, R. G., and Pilling, M. J.: Protocol for the development of the Master Chemical Mechanism, MCM v3 (Part A): tropospheric degradation of non-aromatic volatile organic compounds, *Atmos. Chem. Phys.*, 3, 161–180, doi:10.5194/acp-3-161-2003, 2003.
- 5 Saxena, P., Hildemann, L. M., McMurry, P. H., and Seinfeld, J. H.: Organics alter hygroscopic behavior of atmospheric particles, *J. Geophys. Res.*, 100, 18755–18770, 1995.
- Schnaiter, M., Horvath, H., Möhler, O., Naumann, K.-H., Saathoff, H., and Schöck, O. W.: UV-VIS-NIR spectral optical properties of soot and soot-containing aerosols, *J. Aerosol Sci.*, 34, 1421–1444, 2003.
- 10 Semeniuk, T. A., Wise, M. E., Martin, S. T., Russell, L. M., and Buseck, P. R.: Water uptake characteristics of individual atmospheric particles having coatings, *Atmos. Environ.*, 41, 6225–6235, 2007.
- 15 Shilling, J. E., Chen, Q., King, S. M., Rosenoern, T., Kroll, J. H., Worsnop, D. R., McKinney, K. A., and Martin, S. T.: Particle mass yield in secondary organic aerosol formed by the dark ozonolysis of α -pinene, *Atmos. Chem. Phys.*, 8, 2073–2088, doi:10.5194/acp-8-2073-2008, 2008.
- 20 Shiraiwa, M., Yee, L. D., Schilling, K. A., Loza, C. L., Craven, J. S., Zuend, A., Ziemann, P. J., and Seinfeld, J. H.: Size distribution dynamics reveal particle-phase chemistry in organic aerosol formation, *P. Natl. Acad. Sci. USA*, 110, 11746–11750, doi:10.1073/pnas.1307501110, 2013.
- 25 Suda, S. R., Petters, M. D., Matsunaga, A., Sullivan, R. C., Ziemann, P. J., and Kreidenweis, S. M.: Hygroscopicity frequency distributions of secondary organic aerosols, *J. Geophys. Res.-Atmos.*, 117, D04207, doi:10.1029/2011jd016823, 2012.
- Tolocka, M. P., Jang, M., Ginter, J. M., Cox, F. J., Kamens, R. M., and Johnston, M. V.: Formation of oligomers in secondary organic aerosol, *Environ. Sci. Technol.*, 38, 1428–1434, doi:10.1021/es035030r, 2004.
- 30 Tolocka, M. P., Heaton, K. J., Dreyfus, M. A., Wang, S. Y., Zordan, C. A., Saul, T. D., and Johnston, M. V.: Chemistry of particle inception and growth during alpha-pinene ozonolysis, *Environ. Sci. Technol.*, 40, 1843–1848, doi:10.1021/es051926f, 2006.
- Tost, H. and Pringle, K. J.: Improvements of organic aerosol representations and their effects in large-scale atmospheric models, *Atmos. Chem. Phys.*, 12, 8687–8709, doi:10.5194/acp-12-8687-2012, 2012.

Title Page	Abstract	Introduction
Conclusions	References	
Tables	Figures	
◀	▶	
◀	▶	
Back	Close	
Full Screen / Esc		
	Printer-friendly Version	
	Interactive Discussion	



Relating hygroscopicity and optical properties

C. Denjean et al.

- Tritscher, T., Dommen, J., DeCarlo, P. F., Gysel, M., Barnet, P. B., Praplan, A. P., Weingartner, E., Prévôt, A. S. H., Riipinen, I., Donahue, N. M., and Baltensperger, U.: Volatility and hygroscopicity of aging secondary organic aerosol in a smog chamber, *Atmos. Chem. Phys.*, 11, 11477–11496, doi:10.5194/acp-11-11477-2011, 2011.
- 5 Turpin, B. J. and Huntzicker, J. J.: Identification of secondary organic aerosol episodes and quantitation of primary and secondary organic aerosol concentrations during scaqs, *Atmos. Environ.*, 29, 3527–3544, doi:10.1016/1352-2310(94)00276-q, 1995.
- Vaden, T. D., Song, C., Zaveri, R. A., Imre, D., and Zelenyuk, A.: Morphology of mixed primary and secondary organic particles and the adsorption of spectator organic gases during 10 aerosol formation, *P. Natl. Acad. Sci. USA*, 107, 6658–6663, doi:10.1073/pnas.0911206107, 2010.
- Vaden, T. D., Imre, D., Beránek, J., Shrivastava, M., and Zelenyuk, A.: Evaporation kinetics and phase of laboratory and ambient secondary organic aerosol, *P. Natl. Acad. Sci. USA*, 108, 2190–2195, doi:10.1073/pnas.1013391108, 2011.
- 15 Virtanen, A., Kannisto, J., Kuuluvainen, H., Arffman, A., Joutsensaari, J., Saukko, E., Hao, L., Yli-Pirilä, P., Tiitta, P., Holopainen, J. K., Keskinen, J., Worsnop, D. R., Smith, J. N., and Laaksonen, A.: Bounce behavior of freshly nucleated biogenic secondary organic aerosol particles, *Atmos. Chem. Phys.*, 11, 8759–8766, doi:10.5194/acp-11-8759-2011, 2011.
- 20 Wang, J., Doussin, J. F., Perrier, S., Perraudin, E., Katrib, Y., Pangui, E., and Picquet-Varrault, B.: Design of a new multi-phase experimental simulation chamber for atmospheric photosmog, aerosol and cloud chemistry research, *Atmos. Meas. Tech.*, 4, 2465–2494, doi:10.5194/amt-4-2465-2011, 2011.
- Warren, B., Austin, R. L., and Cocker III, D. R.: Temperature dependence of secondary organic 25 aerosol, *Atmos. Environ.*, 43, 3548–3555, 2009.
- Weingartner, E., Saathoff, H., Schnaiter, M., Streit, N., Bitnar, B., and Baltensperger, U.: Absorption of light by soot particles: determination of the absorption coefficient by means of 30 aethalometers, *J. Aerosol Sci.*, 34, 1445–1463, 2003.
- Wex, H., Petters, M. D., Carrico, C. M., Hallbauer, E., Massling, A., McMeeking, G. R., Poulain, L., Wu, Z., Kreidenweis, S. M., and Stratmann, F.: Towards closing the gap between 35 hygroscopic growth and activation for secondary organic aerosol: Part 1 – Evidence from measurements, *Atmos. Chem. Phys.*, 9, 3987–3997, doi:10.5194/acp-9-3987-2009, 2009.
- Yasmeen, F., Vermeylen, R., Maurin, N., Perraudin, E., Doussin, J. F., and Claeys, M.: Characterisation of tracers for aging of α -pinene secondary organic aerosol using liquid chromatog-

Title Page	
Abstract	Introduction
Conclusions	References
Tables	Figures
◀	▶
◀	▶
Back	Close
Full Screen / Esc	
Printer-friendly Version	
Interactive Discussion	



raphy/negative ion electrospray ionisation mass spectrometry, Environ. Chem., 9, 236–246, doi:10.1071/en11148, 2012.

5 Yu, J. Z., Griffin, R. J., Cocker, D. R., Flagan, R. C., Seinfeld, J. H., and Blanchard, P.: Observation of gaseous and particulate products of monoterpene oxidation in forest atmospheres, Geophys. Res. Lett., 26, 1145–1148, doi:10.1029/1999gl900169, 1999.

Zaveri, R. A., Barnard, J. C., Easter, R. C., Riemer, N., and West, M.: Particle-resolved simulation of aerosol size, composition, mixing state, and the associated optical and cloud condensation nuclei activation properties in an evolving urban plume, J. Geophys. Res.-Atmos., 115, D17210, doi:10.1029/2009jd013616, 2010.

10 Zelenyuk, A., Yang, J., Song, C., Zaveri, R. A., and Imre, D.: A new real-time method for determining particles' sphericity and density: application to secondary organic aerosol formed by ozonolysis of α -pinene, Environ. Sci. Technol., 42, 8033–8038, doi:10.1021/es8013562, 2008.

15 Zhang, Q., Jimenez, J. L., Canagaratna, M. R., Allan, J. D., Coe, H., Ulbrich, I., Alfarra, M. R., Takami, A., Middlebrook, A. M., Sun, Y. L., Dzepina, K., Dunlea, E., Docherty, K., DeCarlo, P. F., Salcedo, D., Onasch, T., Jayne, J. T., Miyoshi, T., Shimono, A., Hatakeyama, S., Takegawa, N., Kondo, Y., Schneider, J., Drewnick, F., Borrmann, S., Weimer, S., Demerjian, K., Williams, P., Bower, K., Bahreini, R., Cottrell, L., Griffin, R. J., Rautiainen, J., Sun, J. Y., Zhang, Y. M., and Worsnop, D. R.: Ubiquity and dominance of oxygenated species in organic aerosols in anthropogenically-influenced Northern Hemisphere midlatitudes, Geophys. Res. Lett., 34, L13801, doi:10.1029/2007gl029979, 2007.

20 Ziermann, P. J. and Atkinson, R.: Kinetics, products, and mechanisms of secondary organic aerosol formation, Chem. Soc. Rev., 41, 6582–6605, doi:10.1039/C2CS35122F, 2012.

25 Zobrist, B., Soonsin, V., Luo, B. P., Krieger, U. K., Marcolli, C., Peter, T., and Koop, T.: Ultra-slow water diffusion in aqueous sucrose glasses, Phys. Chem. Chem. Phys., 13, 3514–3526, doi:10.1039/c0cp01273d, 2011.

Relating
hygroscopicity and
optical properties

C. Denjean et al.

Title Page

Abstract

Introduction

Conclusions

References

Tables

Figures

◀

▶

Back

Close

Full Screen / Esc

Printer-friendly Version

Interactive Discussion



Relating
hygroscopicity and
optical properties

C. Denjean et al.

[Title Page](#)[Abstract](#)[Introduction](#)[Conclusions](#)[References](#)[Tables](#)[Figures](#)[|◀](#)[▶|](#)[◀](#)[▶](#)[Back](#)[Close](#)[Full Screen / Esc](#)[Printer-friendly Version](#)[Interactive Discussion](#)**Table 1.** Initial conditions, temperatures, relative humidities, and results of the experiments.

Experiments	O ₃ ^a (ppb)	Temp (°C)	RH ^b (%)	Mass concentration ^c ($\mu\text{g m}^{-3}$)	Yield ^d
E140910	251	23–25	< 1	130	0.19
E050210	202	19–23	< 1	117	0.18
E080210	232	19–20	< 1	116	0.18
E090210	254	16–17	< 1	118	0.15
E230910	246	22–23	< 1	100	0.17
E160411	232	19–23	< 1	70	0.16
E260411	247	20–25	< 1	—	—
E300911	198	20–27	< 1	78	0.11
E301111	197	18–20	< 1	52	0.07
E091211	196	17–20	< 1	81	0.11
E180411	201	21–26	< 1	86	0.13
E280411	269	17–20	< 1	—	—
E280911	293	22–27	< 1	91	0.13
E021211	196	17–20	< 1	70	0.14
E071211	162	16–19	< 1	55	0.14
E200411	220	21–26	< 1	97	0.15
E260911	292	23–26	< 1	87	0.15
E281111	215	14–19	< 1	44	0.13
E051211	185	16–19	< 1	66	0.13
E120312	229	18–23	< 1	139	0.21
E030512	216	20–23	< 1	109	0.15
E060512	246	19–21	< 1	102	0.16

^a Ozone concentrations determined from FTIR measurement.^b RH before the injection of water at the end of the experiment.^c Aerosol mass concentration estimated from the aerosol volume concentration corrected from dilution and by assuming a density of 1.2 g cm^{-3} .^d Yield calculated from measured aerosol mass and the corresponding concentration of reacted α -pinene, both corrected from dilution. We used the SOA mass concentration and α -pinene concentration after 5 min of reaction as initial concentrations since the initial concentration of α -pinene could not be directly measured.

**Relating
hygroscopicity and
optical properties**

C. Denjean et al.

Table 2. Comparison of real part of the complex refractive index (CRI) of α -pinene-O₃ SOA with previous studies in the literature.

Reference	Real part of the refractive index	λ (nm)
This study	1.32–1.60 (± 0.02)	525
Kim et al. (2010)	1.40–1.50 (± 0.02)	670
Kim and Paulson (2013)	1.39–1.52 (± 0.02)	532
Liu et al. (2013)	1.498 (± 0.002)	550
Nakayama et al. (2010)	1.41 (± 0.02)	532
Nakayama et al. (2012)	1.47–1.48 (± 0.02)	532
Redmond and Thompson (2011)	1.49 (± 0.04)	532
Schnaiter et al. (2003)	1.44	> 350
Wex et al. (2009)	1.45	visible

[Title Page](#)[Abstract](#)[Introduction](#)[Conclusions](#)[References](#)[Tables](#)[Figures](#)[|◀](#)[▶|](#)[◀](#)[▶](#)[Back](#)[Close](#)[Full Screen / Esc](#)[Printer-friendly Version](#)[Interactive Discussion](#)

**Relating
hygroscopicity and
optical properties**

C. Denjean et al.

Table 3. Comparison of size growth factor GF at 90 % RH of α -pinene-O₃ SOA with previous studies in the literature.

Reference	Growth factor (90 %RH)
This study	1.02–1.07 (± 0.02)
Prenni et al. (2007)	1.01–1.07 (± 0.02)
Qi et al. (2010)	1.09
Saathoff et al. (2003)	1.08–1.11 (± 0.01)
Warren et al. (2009)	1.02–1.16 (± 0.02)

[Title Page](#)[Abstract](#)[Introduction](#)[Conclusions](#)[References](#)[Tables](#)[Figures](#)[|◀](#)[▶|](#)[Back](#)[Close](#)[Full Screen / Esc](#)[Printer-friendly Version](#)[Interactive Discussion](#)

**Relating
hygroscopicity and
optical properties**

C. Denjean et al.

Table 4. Comparison of bulk O : C of α -pinene-O₃ SOA with previous studies in the literature.

Reference	Bulk O : C of SOA	Instrumentation
This study	0.55 (± 0.16)–0.68 (± 0.20)	HR-ToF-AMS
Aiken et al. (2007)	0.27 (± 0.08)	HR-ToF-AMS
Shilling et al. (2008)	0.29 (± 0.09)–0.45 (± 0.14)	HR-ToF-AMS
Chhabra et al. (2010)	0.43 (± 0.13)	HR-ToF-AMS
Qi et al. (2012)	0.33	HR-ToF-AMS
Reinhardt et al. (2007)	0.4–0.6	FTICR-MS
Tolocka et al. (2006)	0.37 (± 0.05)–0.40 (± 0.12)	NanoAMS

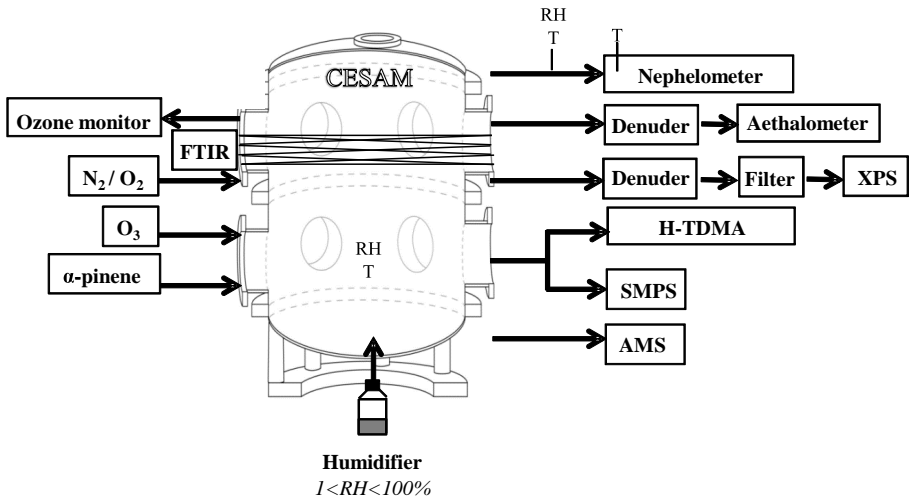


Fig. 1. Experimental set-up of the CESAM chamber used to measure aerosol chemical, hygroscopic and optical properties.

**Relating
hygroscopicity and
optical properties**

C. Denjean et al.

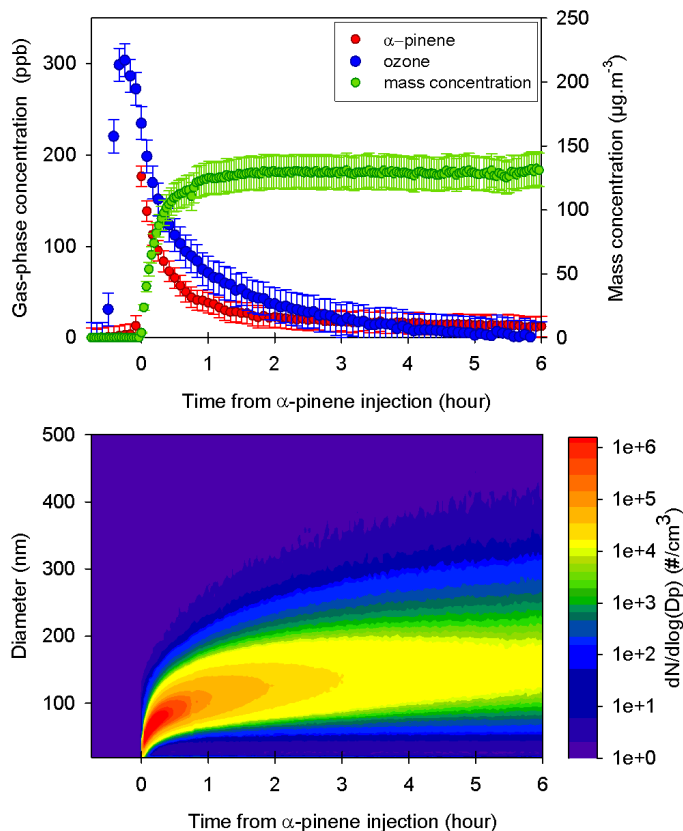


Fig. 2. Temporal profiles of the initial phases of a typical α -pinene ozonolysis experiment (E160410): **(a)** α -pinene (red), ozone (blue) and mass concentration of the SOA (green) and **(b)** measured number size distribution.

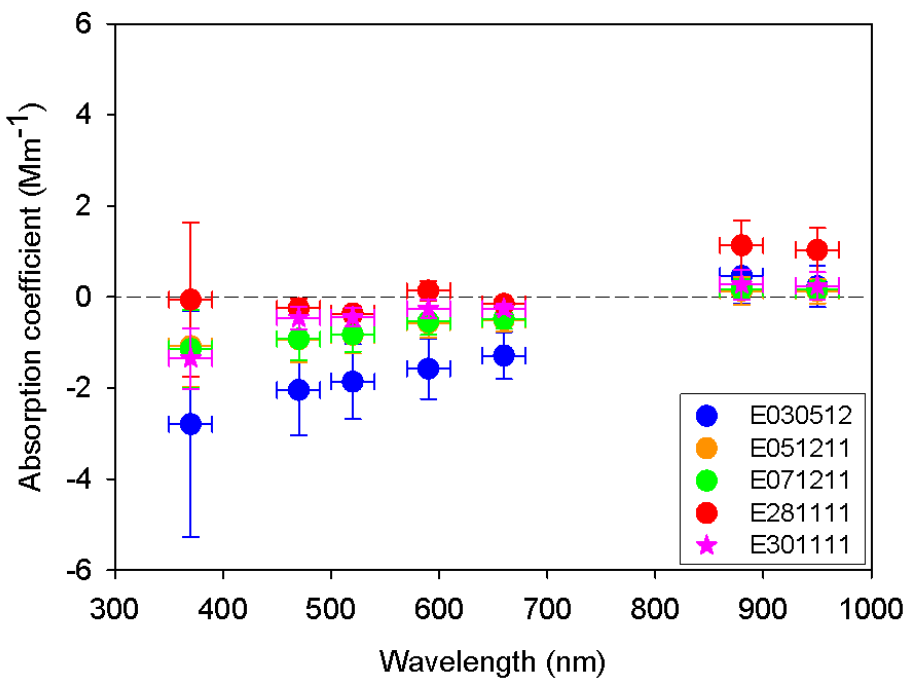


Fig. 3. Wavelength dependence of the spectral absorption coefficients of α -pinene- O_3 SOA after 14 h of reaction.

Relating hygroscopicity and optical properties

C. Denjean et al.

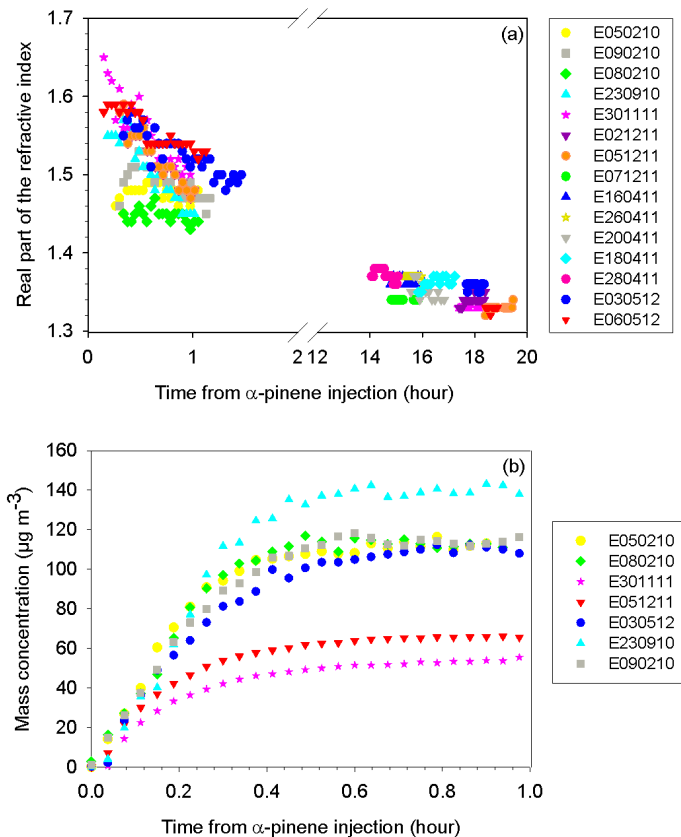


Fig. 4. Calculated real part of the complex refractive index at $\lambda = 525 \text{ nm}$ of SOA as a function of time of reaction (upper panel). The lower panel shows the corresponding mass concentration for the initial formation phase after injection (estimated particle density set to 1.2 g m^{-3}).

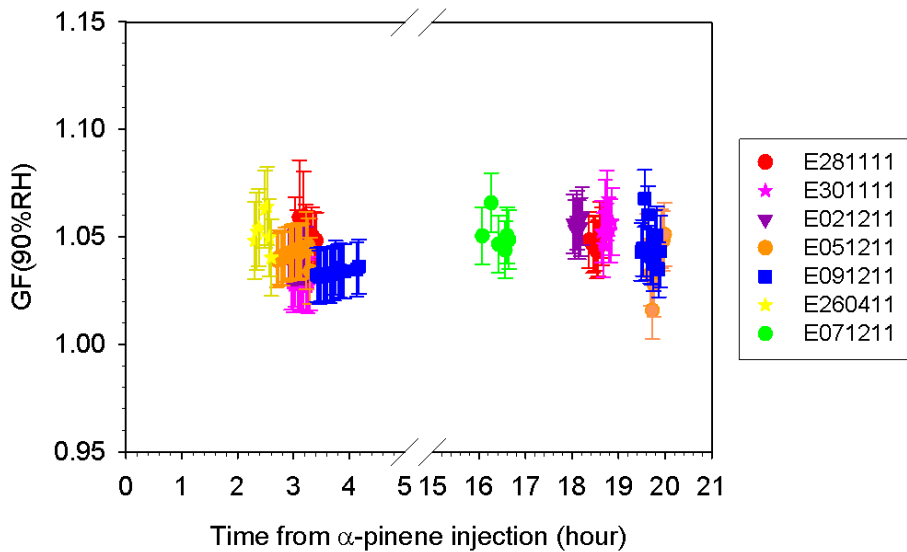


Fig. 5. Size growth factor GF at 90%RH the H-TDMA measurement as a function of time of reaction.

- [Title Page](#)
- [Abstract](#) [Introduction](#)
- [Conclusions](#) [References](#)
- [Tables](#) [Figures](#)
- [◀](#) [▶](#)
- [◀](#) [▶](#)
- [Back](#) [Close](#)
- [Full Screen / Esc](#)
- [Printer-friendly Version](#)
- [Interactive Discussion](#)

**Relating
hygroscopicity and
optical properties**

C. Denjean et al.

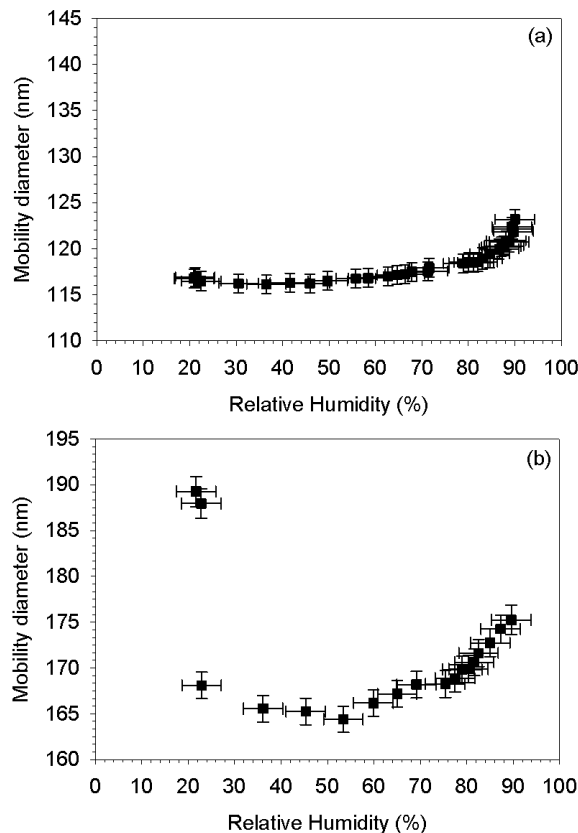


Fig. 6. Mobility diameter as a function of relative humidity measured by the H-TDMA (a) after 1 h reaction for a selected dry size of 115 nm and (b) after 16 h reaction for a selected dry size of 190 nm.

**Relating
hygroscopicity and
optical properties**

C. Denjean et al.

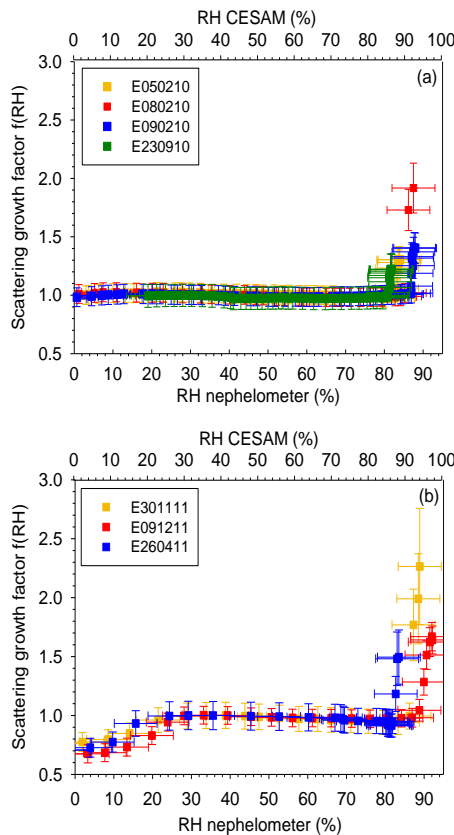


Fig. 7. Change in scattering growth factor as a function of RH within the nephelometer (bottom axis) and the RH within the chamber (upper axis) **(a)** after 1 h reaction and **(b)** after 16 h reaction. The scattering growth factors are calculated as the ratio of σ_{scat} at a specific RH to σ_{scat} at 30 % RH to avoid values lower than 1.

Relating hygroscopicity and optical properties

C. Denjean et al.

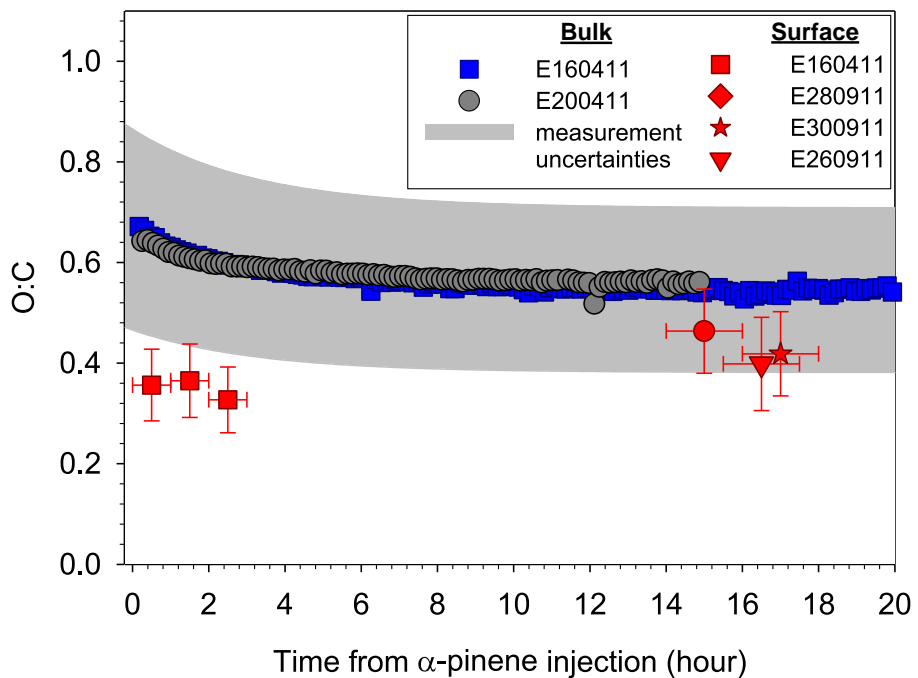


Fig. 8. O : C ratio of the bulk SOA obtained from AMS measurements (blue and grey symbols) and uncertainties in the bulk O : C values (grey area) as a function of time. These bulk O : C ratio are compared with those of the SOA surface determined from XPS analysis (red symbols).

**Relating
hygroscopicity and
optical properties**

C. Denjean et al.

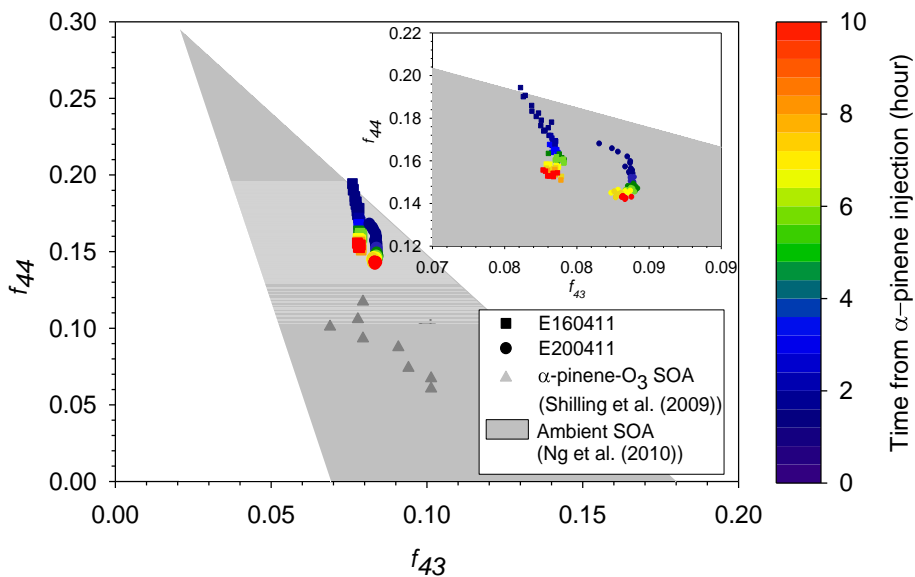


Fig. 9. f_{44} as a function of f_{43} during the α -pinene- O_3 SOA reaction, including experimental data obtained in this study (symbols) and in Shilling et al. (2009), as well as typical ambient SOA (Ng et al., 2010).

- [Title Page](#)
- [Abstract](#) [Introduction](#)
- [Conclusions](#) [References](#)
- [Tables](#) [Figures](#)
- [◀](#) [▶](#)
- [◀](#) [▶](#)
- [Back](#) [Close](#)
- [Full Screen / Esc](#)
- [Printer-friendly Version](#)
- [Interactive Discussion](#)

Relating hygroscopicity and optical properties

C. Denjean et al.

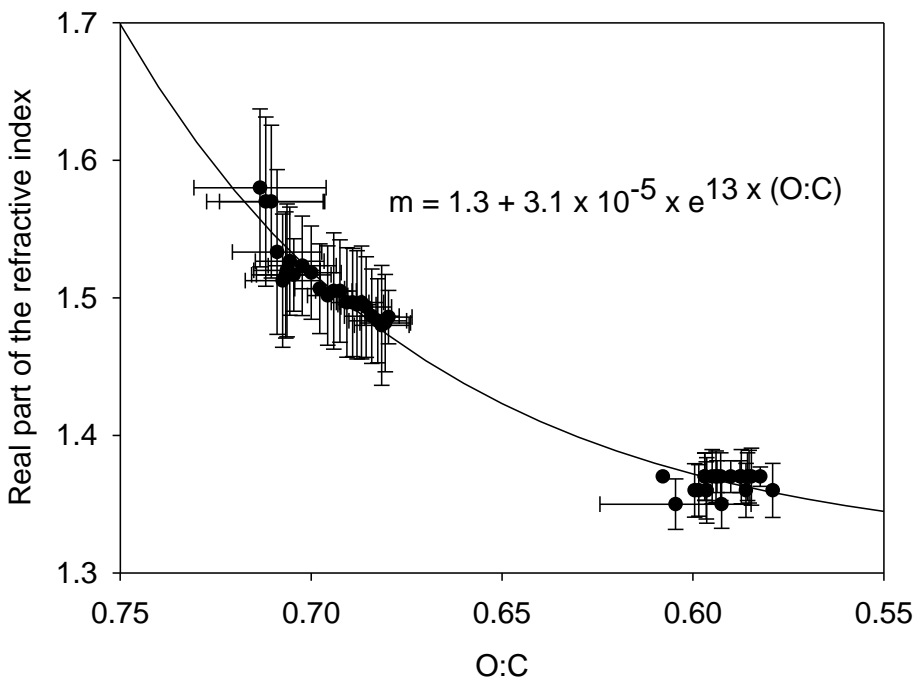


Fig. 10. Real part of the refractive indices of SOA at $\lambda = 525$ nm as a function of O : C bulk ratio. Representative error bars represent $\pm 1\sigma$ in replicate measurement.